UNIVERSITY OF HELSINKI REPORT SERIES IN ASTRONOMY

No. 23

Light scattering in dense particulate media

Timo Väisänen

ACADEMIC DISSERTATION

Department of Physics
Faculty of Science
University of Helsinki
Helsinki, Finland

Doctoral dissertation, to be presented for public discussion with the permission of the Faculty of Science of the University of Helsinki, in Auditorium P674, Porthania building on the 18th of August, 2020 at 12 o'clock.

Helsinki 2020

Cover picture: A sample of dense discrete random media made of samples of Gaussian random spheres.

ISSN 1799-3024 (print version)
ISBN 978-951-51-6119-2 (print version)
Helsinki 2020
Helsinki University Print (Unigrafia)

ISSN 1799-3032 (pdf version)
ISBN 978-951-51-6120-8 (pdf version)
ISSN-L 1799-3024
http://ethesis.helsinki.fi/
Helsinki 2020
Electronic Publications @ University of Helsinki
(Helsingin yliopiston verkkojulkaisut)

Timo Väisänen: **Light scattering in dense particulate media**, University of Helsinki, 2020, 44 p. + appendices, University of Helsinki Report Series in Astronomy, No. 23, ISSN 1799-3024 (print version), ISBN 978-951-51-6119-2 (print version), ISSN 1799-3032 (pdf version), ISBN 978-951-51-6120-8 (pdf version), ISSN-L 1799-3024

Abstract

Physical characterization of planetary objects would be accelerated by the capability of simulating light scattering from an arbitrary dense multiparticle medium. Even though exact methods that solve the Maxwell equations exist, such as the superposition T-matrix method (STMM), they are too compute-intensive to be applied to large macroscale objects such as an asteroid or a planetary surface. Hence, one is to use and develop approximate solutions based on the physics of light scattering.

In the thesis, radiative transfer (RT) based tools are developed, studied, and offered as an approximation to simulate light scattering from dense particulate media. The RT theory has been derived for the sparse random medium, and it fails when applied to the dense random medium. In order to extend the applicability to dense random media, we have been working with the incoherent volume-element treatment for the RT called the radiative transfer with reciprocal transactions ($\mathrm{R^2T^2}$). Instead of using a single particle as the diffuse scatterer in the RT, the properties of the incoherent volume elements are used. These properties are computed from the incoherent electric fields extracted by subtracting the coherent part from the free-space scattered electric fields. The $\mathrm{R^2T^2}$ is validated by simulating various dense random media for which the STMM is still applicable. The comparison between the results computed with the STMM, RT method, and the $\mathrm{R^2T^2}$, show that the $\mathrm{R^2T^2}$ extends the applicability of the RT.

In the geometric optics regime, there are the generalized Snel's law and Fresnel matrices that can be used to simulate light scattering from large objects. For dense particulate media, the computation can be slow, so diffuse scattering as a tool to speed up the computation is studied. Previous studies have included surface roughness with approximate functions, but here a layer of particles is added on top of the diffusely scattering medium. We replace the classical extinction mean free path with more informative extinction distance distribution that is gathered numerically. The comparison between the RT model, our model, and the "ground truth", in which only the generalized Snel's law and Fresnel matrices are used, reveal that our model works better than the RT model.

Even though the computational methods are validated against each other, the methods need to be validated experimentally against controlled samples with well-known physical properties in order to be a reliable source of information. For the validation of the R^2T^2, we computationally simulated a well-controlled sample of which the light-scattering characteristics have been measured. Although the phase function of the simulation and measurement match well, the other scattering characteristics, such as the degree of linear polarization, seem to reveal small discrepancies between the model and the measurements. Still, the various computational validations and this experimental validation show that the R^2T^2 works well and can be used in the near future as a characterization tool.

Acknowledgements

First of all, I want to thank professor Karri Muinonen for wisdom, patience, and trust. I worked in his research project during my doctoral studies, and I am grateful that I got a chance to be part of it. In addition, there are my advisors doctor Johannes Markkanen and doctor Antti Penttilä, to which I am also indebted to for helping me along the way. The university provided the tools, but it was the work done with these three colleagues that taught me to use them. The study presented here was a joint endeavor, but unfortunately, I was the only one who lost his hair.

Thanks to the university, the entire astronomy corridor, and the Planetary-System Research group (past and present members) for creating a pleasant working environment, where I have met some excellent people, such as Erkka Lumme, Joonas Herranen, Julia Martikainen, Lauri Siltala, Olli Ihalainen, and doctor Grigori Fedorets. Special mention to doctor Tomáš Kohout, who has provided a little bit of color to the workplace culture and life in general.

From my friends and relatives alike, I would like to ask forgiveness for not keeping in touch. I want to thank my parents (Ritva & Kalevi), siblings, and grandparents for their support, and my wife Wenyang for looking after me, kicking me, and giving me a perspective of what the normal life is.

I would like to thank professor Ping Yang and professor Tuomo Rossi for pre-examining and commenting on the thesis and doctor Maxim A. Yurkin for agreeing to be the opponent.

Finally, I must acknowledge Google and Stack Overflow: I would not have survived without you.

List of publications

Paper I: Väisänen T., Penttilä A., Markkanen J., Muinonen K., (2016), Validation of radiative transfer and coherent backscattering for discrete random media, *2016 URSI International Symposium on Electromagnetic Theory (EMTS),* 396–399.

Paper II: Muinonen K., Markkanen J., Väisänen T., Peltoniemi J. I., Penttilä A., (2017), Multiple scattering in discrete random media using first-order incoherent interactions, *Radio Science*, 52:1419–1431.

Paper III: Muinonen K., Markkanen J., Väisänen T., Peltoniemi J., Penttilä A., (2018), Multiple scattering of light in discrete random media using incoherent interactions, *Optics Letters*, 43:683–686.

Paper IV: Markkanen J., Väisänen T., Penttilä A., Muinonen K., (2018), Scattering and absorption in dense discrete random media of irregular particles, *Optics Letters*, 43:2925–2928.

Paper V: Väisänen T., Markkanen J., Penttilä A., Muinonen K., (2019), Radiative transfer with reciprocal transactions: Numerical method and its implementation, *PLOS ONE*, 14(1).

Paper VI: Väisänen T., Martikainen J., Muinonen K. (2020), Scattering of light by dense particulate media in the geometric optics regime, *Journal of Quantitative Spectroscopy and Radiative Transfer*, 241.

Paper VII: Väisänen T., Markkanen J., Hadamcik E., Renard J.-B., Lasue J., Levasseur-Regourd A.C., Blum J., and Muinonen K., (2020), Scattering of light by a large, densely-packed agglomerate of small silica spheres, *Optics Letters*, 45:1679–1682.

List of abbreviations

RT	Radiative transfer
CB	Coherent backscattering
RT-CB	Radiative transfer and coherent backscattering
$\mathbf{R^2T^2}$	Radiative Transfer with Reciprocal Transactions
VRTE	Vector radiative transfer equation
GO	Geometric optics
GRS	Gaussian random sphere
GRF	Gaussian random field
STMM	Superposition T-matrix method
MSTM	Multiple Sphere T-matrix method
FaSTMM	Fast Superposition T-matrix method
VSWF	Vector spherical wave functions
SEM	Scanning electron microscope

List of symbols

λ	wavelength
m, m_{re}, m_{im}	complex refractive index and its components
m_{eff}	complex effective refractive index
k	wave number
a	mean radius of a particle
R_V	mean radius of a volume element
R	mean radius of a random medium
$\tilde{\omega}$	single-scattering albedo
v	volume fraction
ℓ	extinction mean free path length
$\mathbf{I}$	Stokes vector
I, Q, U, V	Stokes parameters
$\mathbf{E}$, $\mathbf{E}_{\mathrm{ic}}$, $\mathbf{E}_{\mathrm{coh}}$	free-space, incoherent, and coherent electric field
$\mathbf{B}$	magnetic field
α	phase angle
θ	scattering angle
μ_0, μ	permeability of free space, permeability
ϵ_0, ϵ	permittivity of free space, permittivity
t	time
N	number of particles

Contents

1 Introduction

Remote sensing is a process of measuring characteristics of objects from a distance. Sending a spacecraft to every solar system object is not feasible, and hence the physical characterization of these objects will be based primarily on the remote-sensing data collected by the ground-based or space-based telescopes. The detected feature can be reflectance as the function of the wavelength (spectrum), polarization as the function of the phase angle, or just integrated brightness with specific narrowband or broadband filters. The question is how to link the observed data to the actual characteristics of the object.

In order to interpret the remote-sensing data, the origin of the detected electromagnetic radiation needs to be understood. Some of the observed features are due to the overall geometry and craters (see Fig. 1.1) (Kaasalainen and Torppa, 2001). Some characterization problems need to consider thermal emission (Kolokolova et al., 2004), atmospheric effects (Cottini et al., 2012), or how the loose layer of particulate dust called regolith scatters light (Hadamcik et al., 2011).

Rocky planets, dwarf planets, natural satellites, and small solar system bodies are covered by the regolith (see Fig. 1.1). What is known about the regolith on the astronomical bodies is based on studies of meteorite samples (Cloutis et al., 2014), laboratory studies (Kohout et al., 2014), sample-return missions (Russell and Raymond, 2011; Tsuchiyama et al., 2011), flyby missions (Belton et al., 1992), and the knowledge of the history of the solar system (Pfalzner et al., 2015). Understanding the scattering of light from the regolith is especially crucial for the classification of the asteroids (Tholen, 1989; Bus and Binzel, 2002; DeMeo et al., 2009). The classification is complicated by the effects such as space weathering. The regolith is under constant micrometeorite, solar wind, and cosmic ray bombardment, causing the physical and compositional properties of the exposed regolith to change (Pieters and Noble, 2016). For example, space weathering causes lunar regolith to darken, redden, and to lose distinctive spectral features due to the formed iron nanoparticles (Clark et al., 2002).

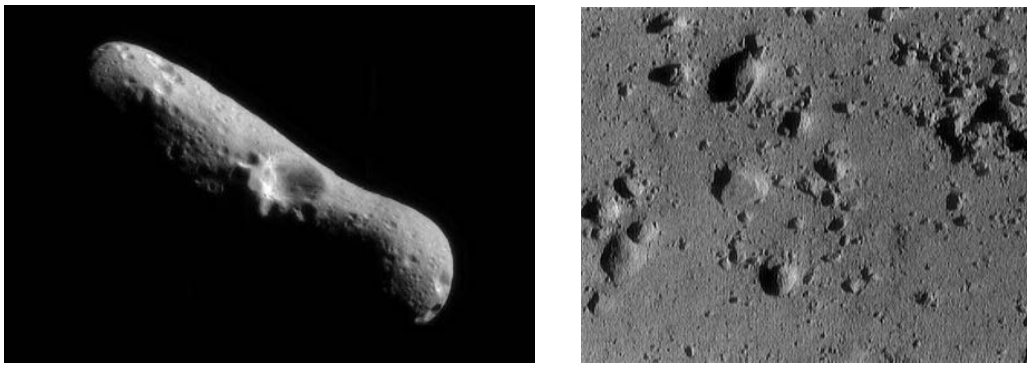

Figure 1.1: Asteroid (433) Eros and its regolith (surface). The images are taken by the NEAR Shoemaker space probe. Image credits: NASA/JPL/JHUAPL and NASA

1.1 Scattering of electromagnetic radiation

Electromagnetic scattering occurs when matter obstructs the propagation of photons. Interaction between these photons that make the electromagnetic radiation and the matter is described by the quantum electrodynamic theory (see, e.g., Cohen-Tannoudji et al., 1989). Fortunately, if the focus is on the elastic scattering of light, absorption, and the propagation, the behavior of electromagnetic radiation can be described accurately by the (macroscopic) Maxwell equations and Lorentz force that make the classical electrodynamics (Griffiths, 2013). They cannot explain the effects such as Raman scattering, fluorescence, spontaneous emission, or thermal emission, but they still offer an adequate theory to be used in engineering and science (Lampe et al., 2003; Chew et al., 2016; Yurkin and Mishchenko, 2018; Chowdhary et al., 2019).

Electromagnetic radiation is a collection of electromagnetic waves. According to the Maxwell equations, the electromagnetic wave is an oscillating electric and magnetic field. It can be characterized by the increasing wavelength of the oscillation from gamma- and X-rays, ultraviolet, visible, and infrared light, to micro- and radio waves. This range of wavelengths or frequencies is called the electromagnetic spectrum. Other characteristics are the amplitude of the oscillating component that is related to the intensity or brightness, whereas the rotation of the plane of oscillation defines the polarization. In elastic light scattering, the wavelength remains the same, meaning that absorbed radiation that is emitted subsequently in different wavelengths is not considered. Still, the brightness and the state of polarization

can change, and they are affected by the physical properties of the scatterer and the incident radiation (Kolokolova et al., 2011; Videen et al., 2015). Fortunately, in planetary science, the primary source of the radiation from ultraviolet to infrared comes from the Sun, which emits unpolarized radiation according to Planck's law of black-body radiation approximately. Alternatively, the incident field can be created artificially with an antenna in the case of radar astronomy. So, when the incident radiation (Sun) and the scattered radiation (observation) is known, the properties of the object can be deduced. This process is called an inverse problem, in which the properties of the object are deduced from the observations by inverting the parameters of a model.

The inverse method is hard because there might be no unique solution, and small errors can cause high inversion errors, not to mention the vast parameter space that has to be analyzed (Aster et al., 2011). Inverse problems rely on the solution of the forward problem. In the forward problem, one tries to experimentally or numerically deduce what should be observed. In the thesis, computational light-scattering methods are developed for the forward problem.

1.2 Modeling the regolith

There are different ways to approach the forward problem of modeling the light-scattering properties of the regolith layer. One of the widely known models in the planetary science community is the Hapke model or the set of Hapke models (Hapke, 1963, 1981, 2008). It has been used to standardize the brightness of the remote-sensing data (Simonelli et al., 1996), and estimate composition (Cruikshank et al., 2001; Mallama et al., 2002). Although the model is useful for standardizing the data, the model has sprouted a debate because it has been deemed to be unphysical as a characterization tool (Shkuratov et al., 2012; Hapke, 2013; Shkuratov et al., 2013). Studies are showing that although it is possible to model some light-scattering properties of the sample using a set of so-called Hapke parameters, these parameters do not reflect their physical counterparts very well, such as the size of the particles or roughness (Shepard and Helfenstein, 2007; Sun et al., 2015).

In the experimental field, researchers create simulant samples that mimic some or all of the observed light-scattering aspects of the regolith. For example, these simulants can resemble lunar, martian, asteroid, or comet samples (CLASS, 2019). The creation of the simulants is not always easy because the environment on the Earth is different that in space. In space, the asteroid regolith is in vacuum, affected by radiation and in low gravity, so the researchers have to invent methods to simulate

the effects such as space weathering in another way (Tang et al., 2012; Kohout et al., 2014).

Finally, there are numerical methods based on the Maxwell equations, which use input parameters that are based on real physical properties such as refractive indices, size and shape distribution, and volume fraction. If a well-controlled laboratory sample is perfectly characterized for simulation and the light-scattering properties are computed by solving the Maxwell equations exactly, the measured light-scattering properties should match the simulated ones. With the simulated database of the different simulant samples, the regolith characterization could be made faster, cheaper, and more reliably. Due to the increased computing capacity of the recent decade, it has been finally possible to simulate light scattering from large and complicated systems (Yurkin et al., 2007; Räbinä et al., 2015; Egel et al., 2017). Unfortunately, the sheer number of objects in the multiparticle systems such as regolith will still make the exact methods inapplicable due to tremendous demand on the computing capacity (Egel et al., 2017). Even though if one manages to simulate the phase function and the polarization accurately for a single wavelength, the simulation needs to be repeated for multiple wavelengths for a spectrum. In order to make multiple-scattering simulations practical, approximations have to be made to cut the complexity of the exact methods. Relevant works about approximations to be used for the physical characterization are from Lumme and Bowell (1981) (a radiative transfer with probabilistic roughness), and Stankevich and Shkuratov (2002) (ray-tracing with geometric optics approximation), to name a few.

1.3 Outline

The main topic of this thesis is the light-scattering computational tools for dense particulate medium using the radiative transfer and especially the radiative transfer with reciprocal transactions. The aim is to develop numerically and experimentally validated computational tools that could be used to characterize a regolith made of arbitrary particles.

In Chapter 2, the relevant theoretical light-scattering concepts are presented briefly. This is followed by Chapter 3, which introduces the computational methods; exact methods, radiative transfer with coherent backscattering (RT-CB), radiative transfer with reciprocal transaction (R^2T^2), and multiparticle SIRIS. In Chapter 4, the applicability of these methods is discussed. Attached Papers I–VII are summarized in Chapter 5 along with the author's contributions. The concluding remarks and prospects are presented in Chapter 6.

2 Theory

2.1 Electromagnetic waves

By following Griffiths (2013), the Maxwell equations can be written in terms of free charges and currents as

$$\begin{aligned} \nabla \cdot \mathbf{D}(\mathbf{r},t) &= \rho_f(\mathbf{r},t), \\ \nabla \cdot \mathbf{B}(\mathbf{r},t) &= 0, \\ \nabla \times \mathbf{E}(\mathbf{r},t) &= -\frac{\partial \mathbf{B}(\mathbf{r},t)}{\partial t}, \\ \nabla \times \mathbf{H}(\mathbf{r},t) &= \mathbf{J}_f(\mathbf{r},t) + \frac{\partial \mathbf{D}(\mathbf{r},t)}{\partial t}, \end{aligned} \tag{2.1}$$

where $\mathbf{H}$ is the magnetic field, $\mathbf{D}$ is the electric field displacement, $\mathbf{B}$ and $\mathbf{E}$ are the magnetic flux density and electric field, ρ_s is the free-charge density, and $\mathbf{J}_f$ is the free-current density. $\mathbf{D}$ and $\mathbf{H}$ are related to $\mathbf{E}$ and $\mathbf{B}$ by constitutive relations that are defined by the properties of the medium in which the field occurs. An important concept for the constitutive relations is electric polarization $\mathbf{P}_b$ and magnetic polarization $\mathbf{M}_b$ that define how the bound electric charges and magnetic dipoles react to the electric and magnetic fields in the medium. For example, in a linear, homogeneous and isotropic medium, $\mathbf{D}$ and $\mathbf{H}$ are written as,

$$\begin{aligned} \mathbf{D} &= \epsilon_0 \mathbf{E} + \mathbf{P}_b = \epsilon_0(1+\chi_e)\mathbf{E} = \epsilon \mathbf{E}, \\ \mathbf{B} &= \mu_0 \mathbf{H} + \mathbf{M}_b = \mu_0(1+\chi_m)\mathbf{H} = \mu \mathbf{H}, \end{aligned} \tag{2.2}$$

where ϵ_0 is the permittivity of free space, χ_e and χ_e are the electric and magnetic susceptibilities, and μ_0 is the permeability of free space.

For a non-magnetic medium (χ_m=0), charge-free (ρ_f=0) and current-free system ($\mathbf{J}_f$=0), Eq. 2.1 can be used to find electromagnetic wave equations

$$\begin{aligned} \nabla^2 \mathbf{E} - \epsilon\mu \frac{\partial^2 \mathbf{E}}{\partial t^2} &= 0, \\ \nabla^2 \mathbf{B} - \epsilon\mu \frac{\partial^2 \mathbf{B}}{\partial t^2} &= 0, \end{aligned} \tag{2.3}$$

that have a solution

$$\begin{aligned}\mathbf{E}(\mathbf{r},t) &= \mathbf{E}_0 \exp(\mathrm{i}\mathbf{k}\cdot\mathbf{r} - \mathrm{i}\omega t),\\ \mathbf{H}(\mathbf{r},t) &= \mathbf{H}_0 \exp(\mathrm{i}\mathbf{k}\cdot\mathbf{r} - \mathrm{i}\omega t).\end{aligned} \tag{2.4}$$

Here, $\mathbf{E}_0$ and $\mathbf{H}_0$ are constant complex vectors, ω is an angular frequency, and $\mathbf{k}$ is a wave vector defines as

$$\mathbf{k} = k(N\hat{\mathbf{e}} + \mathrm{i}K\hat{\mathbf{f}}), \tag{2.5}$$

in which $\hat{\mathbf{e}}$ and $\hat{\mathbf{f}}$ are unit normals to the planes of constant phase and amplitude, N and K are medium-specific apparent refractive indices, and $k{=}2\pi/\lambda$ is a (free-space) wave number defined with a wavelength λ (Bohren and Huffman, 1983; Chang et al., 2005). In addition, there is a complex refractive index m as

$$m = m_{\mathrm{re}} + \mathrm{i}m_{\mathrm{im}}. \tag{2.6}$$

The wave is said to be homogeneous when $\hat{\mathbf{e}}\cdot\hat{\mathbf{f}} = 0$ and inhomogeneous when $\hat{\mathbf{e}}\cdot\hat{\mathbf{f}} \neq 0$, which is the case with a lossy medium. Chang et al. (2005) reports that inhomogeneous waves are required if $m_{\mathrm{im}}/m_{\mathrm{re}}{>}0.01$ and the correct polarization has to be simulated.

In order to make the treatment of the electromagnetic waves easier, in Bohren and Huffman (1983), the electric field is presented with components parallel ($E_\parallel$) and perpendicular ($E_\perp$) to the plane of the propagation,

$$\mathbf{E} = E_\parallel\hat{\mathbf{e}}_\parallel + E_\perp\hat{\mathbf{e}}_\perp, \tag{2.7}$$

which can be even further processed to Stokes parameters with time-averaging for quasi-monochromatic beams,

$$\mathbf{I} = \begin{pmatrix} I\\ Q\\ U\\ V\end{pmatrix} = \begin{pmatrix} \langle E_\parallel E_\parallel^* + E_\perp E_\perp^*\rangle\\ \langle E_\parallel E_\parallel^* - E_\perp E_\perp^*\rangle\\ \langle E_\parallel E_\perp^* + E_\perp E_\parallel^*\rangle\\ \mathrm{i}\langle E_\parallel E_\perp^* - E_\perp E_\parallel^*\rangle\end{pmatrix}. \tag{2.8}$$

The Stokes parameters are the intensity I, linear polarization Q and U, and circular polarization V (see Fig. 2.1). Each of the polarization components define how $E_\parallel$ and $E_\perp$ are related to each other; for example, the sunlight is unpolarized, meaning that the components are $Q{=}U{=}V{=}0$. The Stokes parameters make it easier to interpret measured radiation because traditional optical instruments measure time-averaged squared amplitudes of the fields instead of the instantaneous state of the wave (Mishchenko et al., 2006).

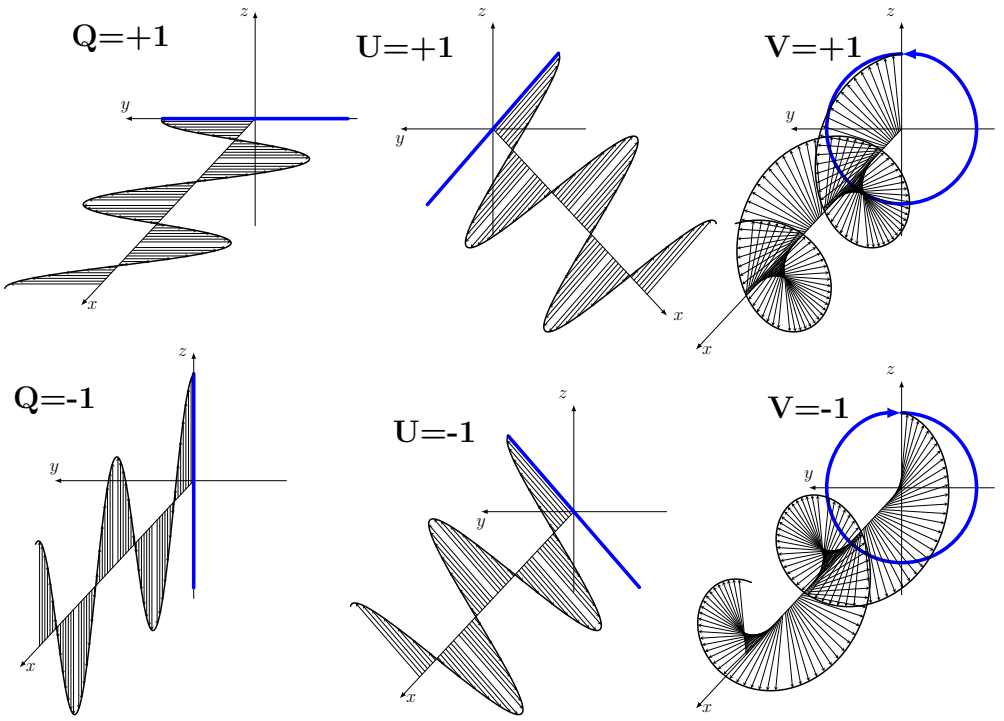

Figure 2.1: Stokes parameters explained visually by drawing the plane of propagation. While Q and U propagate in a plane, the plane of V rotates and thus has a circular pattern. The sign controls the orientation of the plane, whereas intensity I defines the amplitude of the oscillation. For a visual aid, U=-1 propagates in the same direction as U=+1, but the x-axis is shifted to make the pattern more distinctive.

2.2 Light scattering

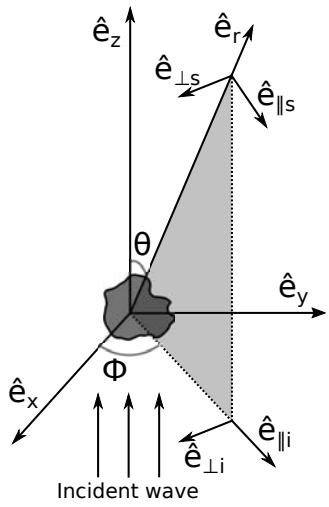

Figure 2.2: Illustration of the incident wave and the scattering plane. (Bohren and Huffman, 1983)

The wave equation itself is not enough to characterize a scattering process. Boundary conditions are used to force a relation between the components of the incident, refracted, and reflected electric and magnetic fields (Bohren and Huffman, 1983; Griffiths, 2013). By defining the incident $\mathbf{E}^{\mathrm{inc}}$ and scattered $\mathbf{E}^{\mathrm{sca}}$ waves in a way presented in Eq. 2.7 and orienting the electric field components as in Fig. 2.2, the relation between the amplitudes in the far field can be written as

$$\begin{pmatrix} E_{\parallel}^{\mathrm{sca}} \\ E_{\perp}^{\mathrm{sca}} \end{pmatrix} = \frac{e^{ikr}}{-\mathrm{i}kr} \begin{pmatrix} S_2 & S_3 \\ S_4 & S_1 \end{pmatrix} \begin{pmatrix} E_{\parallel}^{\mathrm{inc}} \\ E_{\perp}^{\mathrm{inc}} \end{pmatrix}, \tag{2.9}$$

where r is the distance between the scatterer and observer.

For the Stokes parameters, the scattering process is written as

$$\begin{pmatrix} I_{\mathrm{sca}} \\ Q_{\mathrm{sca}} \\ U_{\mathrm{sca}} \\ V_{\mathrm{sca}} \end{pmatrix} = \frac{1}{k^2 r^2} \begin{pmatrix} F_{11} & F_{12} & F_{13} & F_{14} \\ F_{21} & F_{22} & F_{23} & F_{24} \\ F_{31} & F_{32} & F_{33} & F_{34} \\ F_{41} & F_{42} & F_{43} & F_{44} \end{pmatrix} \begin{pmatrix} I_{\mathrm{sca}} \\ Q_{\mathrm{sca}} \\ U_{\mathrm{sca}} \\ V_{\mathrm{sca}} \end{pmatrix} \tag{2.10}$$

in which the 4×4 matrix $\mathbf{F}$ is the scattering matrix. F_{11} is related to the intensity, whereas F_{12}/F_{11} is the degree of linear polarization. The $\mathbf{F}$ can be simplified, because the number of nonzero independent $\mathbf{F}$ elements depends on the symmetries of the scattering medium (van de Hulst, 1981). A thorough study of the scattering matrix is presented in (Hovenier and van der Mee, 1988).

Solving the scattering properties requires a method to solve the $S_{1,2,3,4}$ or $\mathbf{F}$ elements. Electromagnetic scattering can be divided into six boundary regions and the Mie region, which identify available scattering methods to solve them (van de Hulst, 1981). The regimes are distinguished by m_{re} and a size parameter x that is a relation between the radial measure of the scatterer a and k,

$$x = ka = \frac{2\pi a}{\lambda}. \tag{2.11}$$

If the refractive index is intermediate ($m_{\mathrm{re}} \approx 1.5$), there are roughly three regimes: the Rayleigh ($x \ll 1$), Mie/resonance ($x \approx 1$), and geometric optics ($x \gg 1$) regimes. The other four regimes are anomalous diffraction, total reflectors, Rayleigh-Gans, and optical resonance, but these and the Rayleigh scattering are not considered in the thesis.

2.3 *T*-matrix

An alternative way of presenting the electric field (cf. Eqs. 2.7) is

$$\mathbf{E}^{(\nu)} \approx \sum_{v=1}^{N_o} \sum_{w=-v}^{v} (b_{vw1} M_{vw}^{(\nu)} + b_{vw2} N_{vw}^{(\nu)}), \tag{2.12}$$

where $M_{vw}^{(\nu)}$ and $N_{vw}^{(\nu)}$ are base vectors composed of vector spherical wave functions (VSWF, from, e.g., Jackson, 1999) with corresponding coefficients b_{wvu} ($u = 1, 2$). The superscript ν describes how $M_{vw}^{(\nu)}$ and $N_{vw}^{(\nu)}$ are defined. They are either defined by the regular spherical Bessel functions of the first kind or the spherical Hankel functions of the first kind. Finally, N_o is the truncation number that is proportional to the radius enclosing the scatterer. By studying the boundary conditions between the incident (f_{vwu}) and outgoing (a_{vwu}) electric field coefficients, a relation that resembles Eq. 2.9 can be found:

$$\begin{pmatrix} a_{wv1} \\ a_{wv2} \end{pmatrix} = T \begin{pmatrix} f_{wv1} \\ f_{wv2} \end{pmatrix}, \tag{2.13}$$

which includes the so-called transition matrix (T-matrix, Waterman 1965). This T-matrix can be used to present any scattering properties outside a circumscribing sphere provided that the scattering properties can be solved. A downside is that the size of the T-matrix is proportional to the fourth power of N_o, meaning that the solvers require a lot of memory if the size parameter is large (Nieminen et al., 2003).

2.4 Radiative transfer

Phenomenologically, the radiative transfer equation can be derived from the energy conservation (Chandrasekhar, 1960), but a more thorough derivation from the Maxwell equations also exists (Mishchenko et al., 2006), which is briefly summarized here.

By starting from the wave equation (Eq. 2.3), it is possible to derive the so-called Foldy Lax equations (Foldy, 1945; Lax, 1951, 1952), which state that, in the presence of discrete scatterers, the observed electric field $\mathbf{E}$ is a sum of the scattered fields $\mathbf{E}_i^{\mathrm{sca}}$ by N excited particles and the incident field $\mathbf{E}^{\mathrm{inc}}$. The Foldy Lax-equations can be expanded in the order-of-scattering form,

$$\begin{aligned}\mathbf{E} = \mathbf{E}^{\mathrm{inc}} + \sum_{i=1}^{N} \hat{\mathbf{G}}\hat{\mathbf{T}}_i\hat{\mathbf{E}}^{\mathrm{inc}} + \sum_{\substack{i\,=\,1\\ j(\neq i)\,=\,1}}^{N} \hat{\mathbf{G}}\hat{\mathbf{T}}_i\hat{\mathbf{G}}\hat{\mathbf{T}}_j\hat{\mathbf{E}}^{\mathrm{inc}} \\ + \sum_{\substack{i\,=\,1\\ j(\neq i)\,=\,1\\ k(\neq j)\,=\,1}}^{N} \hat{\mathbf{G}}\hat{\mathbf{T}}_i\hat{\mathbf{G}}\hat{\mathbf{T}}_j\hat{\mathbf{G}}\hat{\mathbf{T}}_k\hat{\mathbf{E}}^{\mathrm{inc}} + ...,\end{aligned} \tag{2.14}$$

in which $\hat{\mathbf{G}}\hat{\mathbf{T}}_i$ are operators that describe how the electric field is scattered by the particle i. Simply, Eq. 2.14 states that the scattered field $\mathbf{E}^{\mathrm{sca}}$ is the sum of the "single-scattered", "double-scattered", "triple-scattered" fields, and so forth. Eq. 2.14 is challenging to solve exactly for a multiparticle system with a large N, and hence, various approximations have to be applied.

The first simplification states that the particles are located in the far-field zones of each other, which simplifies the operators $\hat{\mathbf{G}}$ and $\hat{\mathbf{T}}$ because the particles see each other as point sources. The far-field approximation can be applied further and used to omit self-excitations (see in Fig. 2.3), which reduces the number of possible scattering paths. This is called the Twersky approximation (Twersky, 1964).

Now the radiative transfer equation can be derived for a sizeable ergodic medium by studying the dyadic correlation function, in which $\mathbf{E}$ is multiplied with itself by dyadic product and averaged over all the configurations. In order to simplify the correlation function, certain interacting scattering paths that are visualized in Fig. 2.3 have to be removed. The first approximation removes products of scattering paths that have no common scatterers because the averaging causes them to cancel out due to oscillations. Now products of paths that have at least one common scatterer are left. Next, the ladder approximation is applied that removes all the paths, which do not share the same paths (see Fig. 2.3). These other paths are again canceled out due to the oscillations during the averaging.

With these approximations, it is possible to derive the vector radiative transfer equation (VRTE), which describes the observed electric field from a large, sparse, ergodic medium such as atmosphere or interstellar gas cloud. It is a sum of diffusively scattered waves that are affected by exponential extinction, and a separate coherent part.

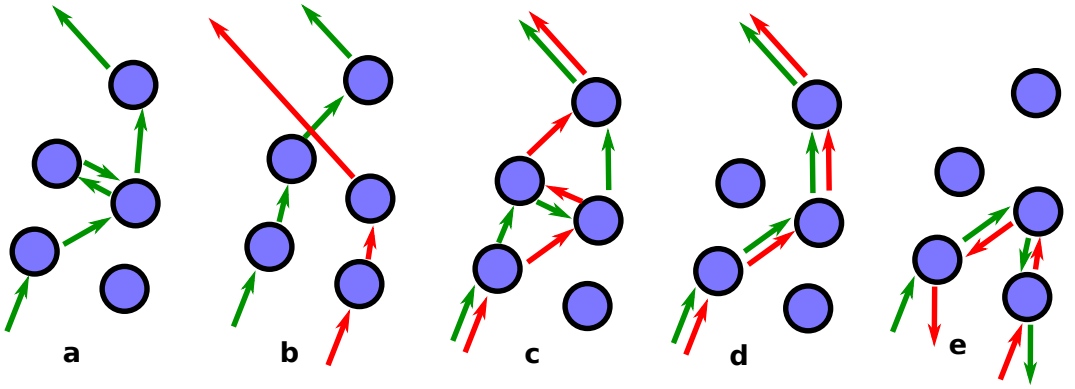

Figure 2.3: Visualization of the electric field paths that appear during the derivation of the VRTE: Paths in which the same particle excites itself are removed in the Twersky approximation (a); Dyadic product of paths with no connectors cancels out when the number of particles approaches infinity (b); The dyadic products that cancel out due to averaging during the ladder approximation (c). The dyadic products that are left after all the approximations (d); Finally, the crossing connectors that cause coherent backscattering, but which are omitted due to the ladder approximation (e).

2.5 Coherent backscattering

The ladder approximation in Sec. 2.4 omits an important phenomenon observable near the backscattering direction called coherent backscattering (CB) that causes an intensity spike and negative polarization surge. The ladder approximation removes cyclical diagrams that cause constructive interference between two waves traveling in opposite directions which is especially prominent near the backscattering angles (see Fig. 2.3) (Mishchenko et al., 2006). The phase difference between these waves can be accounted for by using the equation

$$\Delta\phi = k(\hat{\mathbf{k}}_f + \hat{\mathbf{k}}_i) \cdot (\mathbf{r}_n - \mathbf{r}_0), \tag{2.15}$$

in which $\hat{\mathbf{k}}_f$ and $\hat{\mathbf{k}}_i$ are the directions of the scattered and incident field, and $\mathbf{r}_n$ and $\mathbf{r}_0$ are the positions of the last and first scatterers in the light-scattering path. The phase difference vanishes when $\mathbf{k}_f = -\mathbf{k}_i$, meaning that the two waves are interfering constructively. The CB has been added to the Monte Carlo RT solution by computing the interference of the cyclical diagrams separately (Muinonen, 2004). Fig. 2.4 shows the difference between the RT only and the RT-CB solution.

In astronomy, one of the phenomena that was not fully understood before was the brightening and the polarization surge of the object in the backscattering direction

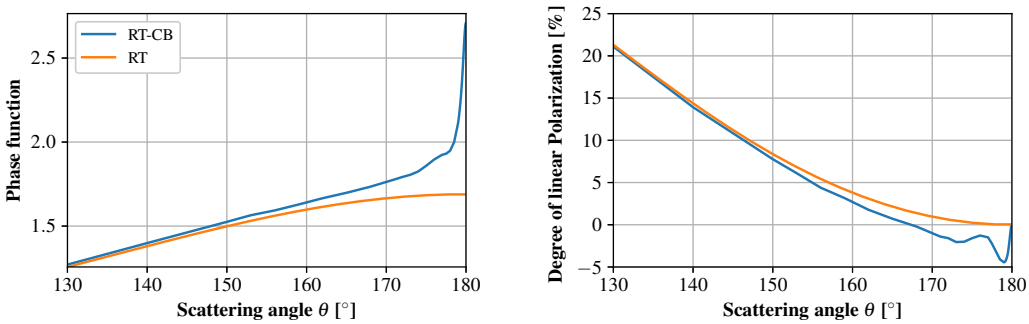

Figure 2.4: An example of a case in which pure RT solution is compared against the RT with the added CB effect.

when the Sun, observer, and the Moon are aligned in opposition. The Moon is then roughly twice as bright as it was the day before (Gehrels et al., 1964). The shadowing mechanism was thought to be the leading cause for the brightening (Hapke, 1963), but for now, the CB has been accepted as at least a partial the explanation for it (Shkuratov, 1988; Muinonen, 1990; Hapke et al., 1993; Muinonen et al., 2011). The brightening is not only observed for the Moon, but for Saturn's rings (Seeliger, 1887) and asteroid surfaces (Gehrels et al., 1964), too.

2.6 Incoherent fields

The VRTE has a diffuse and coherent part (Mishchenko et al., 2006). Coherent radiation is transformed into the diffuse radiation while traversing the medium, and in order to separate them from each other, incoherent fields can be used (Tsang and Ishimaru, 1987; Tsang et al., 1992; Zurk et al., 1996).

The scattered electric field $\mathbf{E}_i^{\mathrm{sca}}$ of the realization i can be decomposed into the incoherent field $\mathbf{E}_i^{\mathrm{sca,ic}}$ and the coherent field (mean or ensemble-averaged field) $\mathbf{E}^{\mathrm{sca,c}}$,

$$\mathbf{E}_i^{\mathrm{sca}} = \mathbf{E}_i^{\mathrm{sca,ic}} + \mathbf{E}^{\mathrm{sca,c}}. \tag{2.16}$$

The coherent field is the average over all the possible realizations:

$$\mathbf{E}^{\mathrm{sca,c}} = \lim_{N_{\mathrm{r}}\to\infty} \frac{1}{N_{\mathrm{r}}} \sum_{i=1}^{N_{\mathrm{r}}} \mathbf{E}_i^{\mathrm{sca}}. \tag{2.17}$$

With the coherent field, the incoherent electric field can be extracted from Eq. 2.16 with a simple subtraction.

Now it is important to notice that the first moment of the incoherent field is:

$$\langle \mathbf{E}^{\mathrm{sca,ic}} \rangle = 0, \tag{2.18}$$

but the second moment is non-zero:

$$\langle |\mathbf{E}^{\mathrm{sca,ic}}|^2 \rangle = \langle |\mathbf{E}^{\mathrm{sca}}|^2 \rangle - |\mathbf{E}^{\mathrm{sca,c}}|^2. \tag{2.19}$$

This leads to a relation

$$\langle |\mathbf{E}^{\mathrm{sca}}|^2 \rangle = \langle |\mathbf{E}^{\mathrm{sca,ic}}|^2 \rangle + |\mathbf{E}^{\mathrm{sca,c}}|^2, \tag{2.20}$$

that states that the second moment of the free-space scattered field decomposes into the incoherent and coherent components.

2.7 Gaussian random sphere

Simulating light scattering from a particulate medium requires a method to generate particles. In Grynko et al. (2016), the particles were created by extracting them from the Gaussian random field. Another method is to generate samples of Gaussian random spheres (GRS) that represent irregular particles with well defined statistical properties (see Fig. 2.5) (Muinonen et al., 1996; Peltoniemi et al., 1989) and they have been used in numerous studies as in Volten et al. (2001), Martikainen et al. (2018), Lindqvist et al. (2018), Markkanen et al. (2018), and Martikainen et al. (2019) to name just a few.

GRS particles can be generated from a set of equations,

$$\begin{aligned} r(\theta,\phi) =& \frac{a \exp(s(\theta,\phi))}{\sqrt{1+\sigma^2}}, \\ s(\theta,\phi) =& \sum_{l=0}^{\infty} \sum_{m=-l}^{l} s_{lm} Y_{lm}(\theta,\phi), \end{aligned} \tag{2.21}$$

where σ is the relative standard deviation of the radial distance, $s(\theta,\phi)$ is the logarithmic radial distance, Y_{lm} are the orthonormal spherical harmonics, and s_{lm} are Gaussian random variables with zero means. The values of $s(\theta,\phi)$ over the full solid angle are controlled by a covariance function, which is defined with a series of Legendre polynomials.

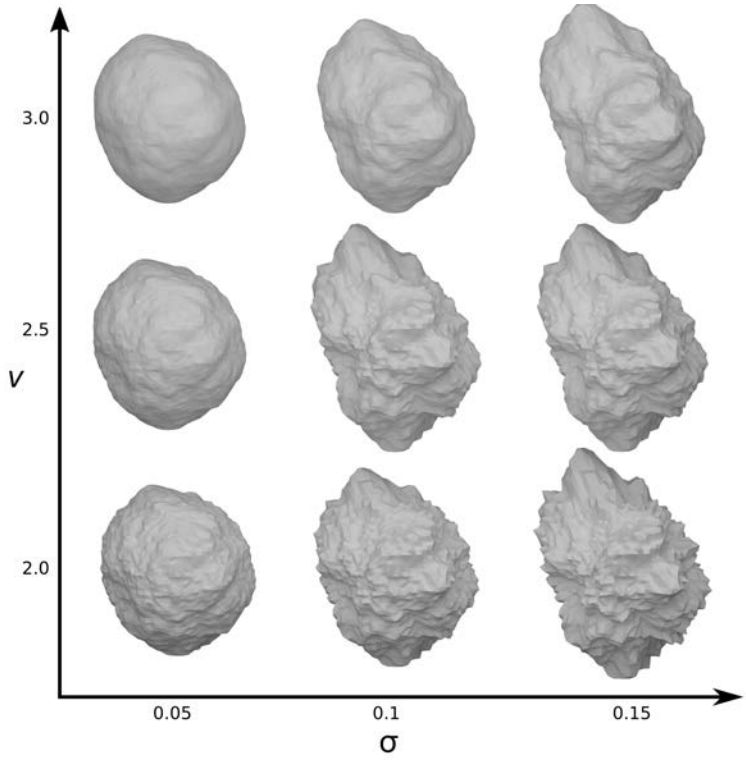

Figure 2.5: GRS particles generated with different radial standard deviation σ and the power-law index ν both of which control the statistical shape. The same seed for the random number generator is used in each case.

3 Computational methods

3.1 Exact methods

Various exact theoretical methods can solve the Maxwell equations numerically. Each method has its limitations, so there is no single method that is applicable everywhere. In the attached papers, we have used the Lorenz-Mie method, the Superposition T-matrix method (STMM), and the volume integral equation method (VIEM).

Lorenz-Mie theory (van de Hulst, 1981; Bohren and Huffman, 1983) can be used to solve the single scattering from a sphere or multilayered sphere (Babenko et al., 2003). Because it offers an exact presentation of the scattering from a sphere, it is a widely used method when single scattering from a spherical particle is considered. In the theory, the incident, internal, and scattered fields are presented with VSWFs in a similar way to that in Sec. 2.3, and the coefficients of the field are solved by applying boundary conditions.

The superposition T-matrix method (STMM, Bruning and Lo, 1971a,b; Peterson and Ström, 1973) is an exact method that can solve light scattering by a multiparticle medium. In STMM, the light-scattering properties of particles are presented with the T-matrices (see Sec. 2.3), and the method solves the interaction between them. The T-matrices can describe arbitrary particles, meaning that the single-scattering characteristics can be solved separately from the multiple scattering problem. The STMM software used in the attached papers are Multiple sphere T-matrix (MSTM 3.0, Mackowski and Mishchenko, 2011) method and Fast superposition T-matrix method (FaSTMM, Markkanen and Yuffa, 2017).

Finally, VIEM was used with the electric current volume integral equation solver JVIE (Markkanen et al., 2012) to solve the light scattering by irregular particles. JVIE uses the method of moments for geometries that are discretized with tetrahedral elements (see Fig. 3.1), and is the slowest of the methods discussed above. The method can solve the T-matrix, which then can be applied to the multiple scattering computation with FaSTMM or $\mathrm{R^2T^2}$. The method was used in Paper IV and VII to solve the multiple-scattering and single-scattering properties of irregular particles.

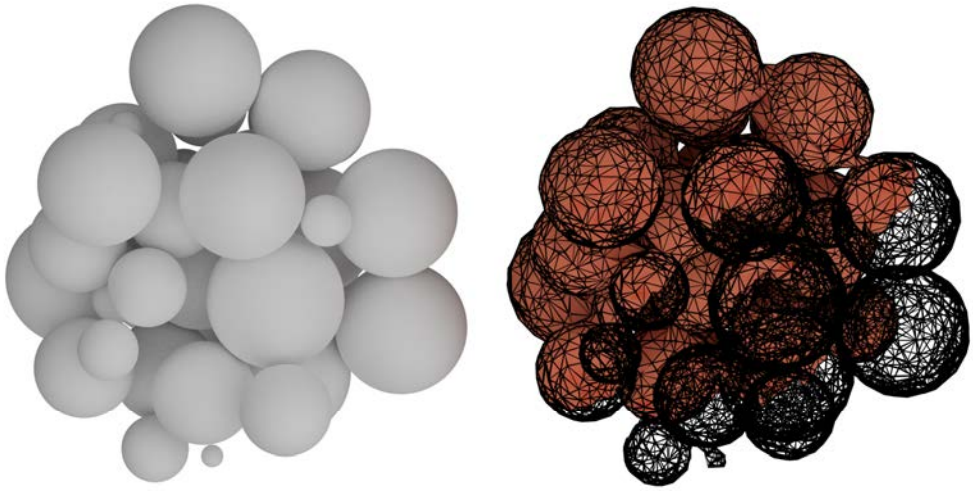

Figure 3.1: A visual presentation of the volume elements that can be used as input for the STMM (left) and JVIE (right). The volume element in the right consists of tetrahedral elements with bridges between the particles.

Spherical media is considered in all of the validations in Papers I-V because it makes it possible to model discrete random media exactly with the STMM without approximation about the semi-infinite layer. It is also faster because orientation averaging can be used to accelerate the convergence of the results obtained with the STMM methods.

3.2 SIRIS

SIRIS is a geometric optics ray tracer for GRS particles (Muinonen et al., 1996, 2009). The original version used the classical Snel's law and Fresnel reflection and refraction matrices, and later the diffuse scattering capabilities were implemented.

In the classical sense, the phases of the electric fields are homogeneous, but when absorption is present the amplitude and phase vector ($\hat{\mathbf{e}} \cdot \hat{\mathbf{f}} \neq 0$, see Eq. 2.5) are not parallel and the field is inhomogeneous (Epstein, 1930). This causes an error to the simulation in a strongly absorbing medium if the inhomogeneous waves and proper treatment (generalized Snel's law, Dupertuis et al., 1994a) are neglected (Chang et al., 2005). The inhomogeneous waves were incorporated into the newer SIRIS4 (Lindqvist et al., 2018) to study the absorption of the ice crystals, and later diffuse scattering properties were added to study the multiple scattering from a regolith

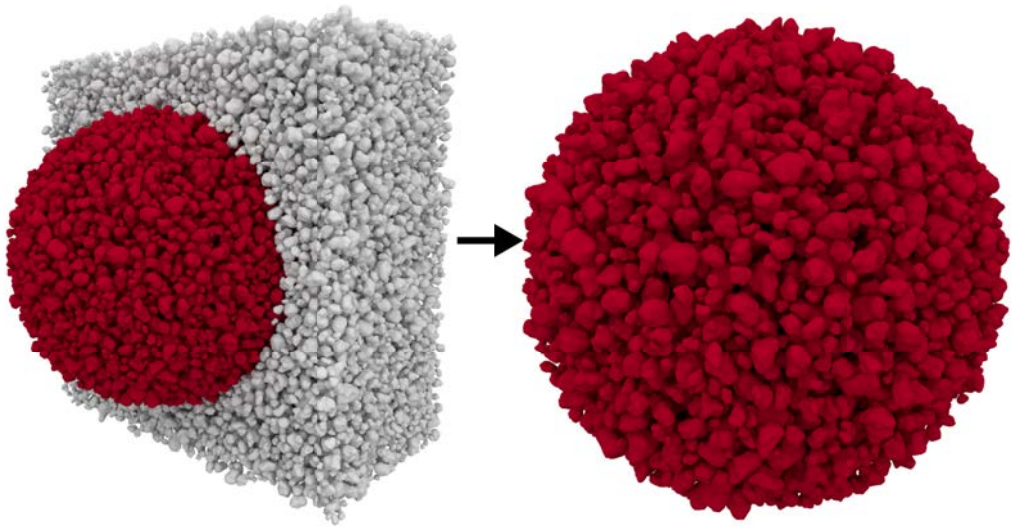

Figure 3.2: Spherical volume element is culled from a periodic box.

(Martikainen et al., 2018). There are also other implementations of ray-tracers with inhomogeneous waves by Yang et al. (2001) and Yang and Liou (2009).

In the latest iteration of the SIRIS (see Paper VI), the software was written to support any shapes, multiple particles, and materials. The most considerable differences between SIRIS and the RT-CB are that the RT-CB can compute the CB, the convergence is accelerated with the peel-off technique, and the RT-CB does not have any geometric optics capabilities.

In SIRIS, the multiple rays are generated outside the medium within given parameters (direction, and location). The rays are traced to the surface of the first intersecting triangle, where the ray can split to the refracted and reflected rays according to the generalized Snel's law and the material properties. If the ray enters a diffuse medium, the ray is allowed to scatter diffusely and change direction while traversing within it. In the absorbing medium, the absorption is applied to the ray, and if the intensity of the ray drops below the given cutoff limit, the ray is killed. When the ray intersects another triangle, the ray splits to the refracted and reflected rays again, until they intersect nothing and are collected. The splitting of the rays makes the method slow for the particulate medium and can cause convergence issues due to various rays reaching the cutoff limit prematurely. Another problem is that the rays might never exit the medium. To speed up SIRIS, the rays are allowed to

split up to a certain order, after which they can only refract or reflect.

The latest iteration of SIRIS requires meshes that are used to present the scattering medium, and for that purpose, we implemented a simplified version of the mechanical contraction from Williams and Philipse (2003); de Lange Kristiansen et al. (2005); He et al. (2000) to generate meshes that resemble a dense random particulate medium for Paper VI. Initially, the particles are randomly placed inside a periodic box, which is then shrunk periodically until the desired volume fraction is achieved. Different geometries can be extracted from the periodic box by culling (see Fig. 3.2).

3.3 Radiative Transfer with Coherent Backscattering

Radiative Transfer with Coherent Backscattering (RT-CB) is an approximate method, which solves the radiative transfer equation and coherent backscattering (see Secs. 2.4 and 2.5, Muinonen, 2004). The RT-CB uses Monte Carlo integration to solve the VRTE by tracing rays, each of which has its wave properties presented with the Stokes parameters (see Eq. 2.8). Alongside the Stokes parameters, the corresponding electromagnetic wave (see Eq. 2.7) is traced and used for the CB computation.

The RT-CB solves the scattering matrices by generating multiple rays with different Stokes parameters and tracing them within the diffuse medium. These rays are traced from point to point where they are affected by a diffuse scatterer that changes the direction according to the equation that resembles the solution of the Kepler equation (Muinonen, 2004). In the simplest ray-tracing model, the rays would be collected when they exit the medium, which is a slow approach. However, the RT-CB uses the so-called peel-off strategy that accelerates the convergence (Yusef-Zadeh et al., 1984), in which each diffuse scattering event generates additional rays that are traced outside the medium and collected, if possible. The collected flux is then subtracted from the original ray, and the ray traverses and diffusely scatters within the medium until its flux drops below some user-defined limit. Additionally, after each diffuse scattering event, the CB part is computed by tracing another ray but in reverse order (see Fig. 2.3), which then interferes with the original ray.

Compared to the multiple scattering exact methods presented in Sec. 3.1, the RT-CB is far less compute-intensive and can be run on a single processor. The modernized version of the RT-CB (Paper I) was written as the framework for the early version of the R^2T^2 (see Sec. 3.4, Muinonen et al., 2016).

3.4 Radiative Transfer with Reciprocal Transactions

The Radiative Transfer with Reciprocal Transactions (R^2T^2, Papers II–V) extends the applicability of the RT-CB to dense random media by incorporating the use of the incoherent interactions to the RT. In Sec. 2.6, it was shown that the second moment of the scattered field could be decomposed into the coherent and incoherent parts. Now, the incoherent component can be approximated by using the RT theory, with a distinction that incoherent volume elements are used as a diffuse scatterer with the incoherent fields and the corresponding relations (incoherent extinction mean free path, incoherent single-scattering albedo).

The incoherent volume elements are small multiparticle partitions of the studied medium. Incoherent volume elements are generated by creating various realizations of volume elements, for which light-scattering characteristics are computed with the exact methods. Then these light-scattering characteristics can be used to extract the incoherent light-scattering properties (see Eqs. 2.16 and 2.17). For the R^2T^2, the incoherent volume elements are computed with the modified version of the FaSTMM or JVIE and their scattering properties are saved in the T-matrices that can be used in the R^2T^2.

The R^2T^2 solves the RT in the RT in the same way as the RT-CB. The essential difference is that it solves the interaction between the incoherent volume element and the electric field rigorously using the T-matrix method (see Sec. 2.3). This makes the R^2T^2 compute-intensive but also memory demanding due to all the T-matrices that present the incoherent volume elements.

Simpler versions of the R^2T^2 have been developed. The first approximation is to use the first-order scattering to form the average incoherent volume element. The phase functions of the volume elements were generated by placing particles inside a volume element, and then the incoherent first-order characteristics were solved with the Mie theory. These volume elements were then averaged and used to extract the incoherent scattering characteristics and their averaged properties. The average incoherent volume element is then used as input for the RT-CB (see Paper II). We call the procedure as the first-order R^2T^2. The first-order-scattering approximation cuts the time consumption from the precomputations part and also from the final computations.

There is also a version of the R^2T^2 that uses the averaged scattering matrices (Markkanen et al., 2018) instead of the T-matrices, which was also applied in Paper VII. This is the simplified R^2T^2, in which the averaged incoherent scattering characteristics are solved, and used as a diffuse scatterer in the RT capable software, such as SIRIS. The problem with this is that the asymmetrically scattering volume

elements cannot be presented with the averaged scattering matrices, and how to implement the CB. The benefit of using the SIRIS is that the effects of the coherent component can be approximated with the laws of the geometric optics (Markkanen et al., 2018).

The coherent effects are caused by collective scattering and interaction with the matter that is not present in the R^2T^2. These effects were included in the RT model in Markkanen et al. (2018) with the mean-field correction by following Zurk et al. (1996). The incident rays that interact with the surface of the medium can be refracted and reflected according to the generalized Snel's law (Dupertuis et al., 1994b; Chang et al., 2005) by using an effective refractive index m_{eff} that needs to be generated with a separate procedure. First the free-space scattering cross-section (C_{sca}) of the volume element (R_V) was simulated alongside the incoherent extinction cross-section ($C_{\text{ext}}^{\text{ic}}$). Next, C_{sca} was matched with the free-space scattering cross-section of the circumscribing sphere with a radius R_V obtained from Lorenz-Mie by adjusting the m_{re} that would act as a real part of the effective refractive index m_{eff}. Then, the imaginary part of m_{eff} can be computed from

$$\text{Im}(m_{\text{eff}}) = \frac{3C_{\text{ext}}^{\text{ic}}}{(8\pi k R_V^3)}. \tag{3.1}$$

4 Extension to dense media

4.1 Radiative transfer for dense media

The RT theory is derived for the ergodic, sparse, and large medium, and hence, it will likely fail when applied outside the range of the applicability (Mishchenko et al., 2006). Still, the RT-CB works relatively well when applied to a small medium (kR=40) with modest numbers of particles (N=250 and 500), as was shown in Muinonen et al. (2012). A similar study was conducted later in Paper I with a larger medium ($kR \approx$[47, 86]) and higher densities to test the limits of the RT-CB. In the study, the number of particles (m=1.31, ka=2) was kept constant (N=4000), but the volume fraction v of the medium was varied from 0.05 to 0.3. The light-scattering properties were then simulated with the RT-CB (see Sec 3.3) and the MSTM (see Sec. 3.1). The comparison strengthened the claim in Muinonen et al. (2012) that the RT-CB works relatively well with a sparse small-sized medium but failed when the density grew, as expected.

Trying to extend the applicability of the RT to dense random media is not a new idea (Tsang et al., 1985; Tsang and Ishimaru, 1987). Ishimaru and Kuga (1982) have shown that scattering in a dense system is correlated between the scatterers, and hence the independent scattering is not a valid assumption. There exists a couple of methods that extend the applicability of the RT to dense media, such as the quasi-crystalline approximation (QCA), the quasi-crystalline approximation with coherent potential (QCA-CP), and the dense media radiative transfer theory (DMRT) (Tsang et al., 2001). In these methods, near-field coherent field interactions are included, and the Percus–Yevick approximation to the pair distribution function is used to account for the particle positions in the dense media (Tsang et al., 2001). The QCA and QCA-CP have been shown to work for dense media consisting of spherical particles, but the QCA-CP is limited to small particles (Tsang et al., 2000). DRMT is derived from QCA and works for moderate-sized particles and sticky particles (Tsang et al., 2001). More recent works to approximate the multiple scattering from dense particulate media are by Ito et al. (2017) and Ramezanpour and Mackowski (2019).

In the R^2T^2, the applicability is extended by the use of the incoherent fields. Correlation and the near-field scattering effects are considered inside the incoherent volume element, whereas the contribution of the entire element affects other volume elements via the incoherent fields the same way as the diffuse parts in the RT theory. The use of the dense volume elements violate the far-field and the independent scattering assumptions in the RT theory, but the R^2T^2 still relies heavily on the aspects of the RT such as diffuse scattering and exponential attenuation.

In order to test the validity of the R^2T^2, dense discrete random media were simulated using the MSTM, the R^2T^2, and the RT-CB. The initial results were promising, but the R^2T^2 could not simulate the absolute level of the intensity, and the coherent backscattering parts were missing (Muinonen et al., 2016). Later, a study with the incoherent first-order scattering in Paper II revealed that the original R^2T^2 results were affected by incorrect statistics of volume elements. In Paper II, the forward-scattering direction of the averaged phase function was corrected semi-empirically, but it turned out that, if the statistics were correct, this step was unnecessary. The volume elements should be culled from a large periodic box that has correct statistics. The R^2T^2 was tested again by simulating two dense random media (kR=100, v=0.15 and 0.30, m=1.31), and comparing them against the FaSTMM results revealed that the R^2T^2 performed well (Paper III). The R^2T^2 produced similar phase function and degree of linear characteristics as the FaSTMM that RT-CB was not capable of producing. In order to give a perspective of the time usage and the need for the approximations such as R^2T^2, the exact computations of the kR=100 case in Paper III would take around nine months to complete in serial CPU time, whereas the R^2T^2 took around a week in serial CPU time.

Later, the R^2T^2 was applied to compute scattering from a medium consisting of irregular particles in Paper IV. This was achieved with the JVIE that is capable of solving the light-scattering characteristics of the tetrahedral elements and create corresponding T-matrices that can be used in the R^2T^2. The last computational validation with different configurations and the thorough explanation of the R^2T^2 are presented in Paper V, which also studied the extinction coefficients and albedos of the volume elements.

Even though the results simulated with the R^2T^2 and FaSTMM match with each other relatively well, there exist one major open question studied in Paper V that needs to be addressed in order to make the method more robust. The R^2T^2 has one free parameter, which is the radius of the volume element. The radius of the volume element affects the extinction mean free path, and, in that way, also the absolute level of the intensity and the degree of linear polarization. The problem is connected to the exponential attenuation model derived for the sparse medium that controls

the attenuation within the medium. In order to find a better attenuation model, the electric fields inside the dense discrete random media should be studied.

In order to improve the R^2T^2, coherent effects (see Sec. 3.4) should be included that refract rays when they enter the medium. In Markkanen et al. (2018), the coherent effects were added to the simplified version of the R^2T^2 by following Zurk et al. (1996). The simplified version of the R^2T^2 was achieved by using the SIRIS program with incoherent averaged scattering matrices that can refract rays, which, on the other hand, lacks the CB capabilities.

4.2 Diffuse scattering in the geometric optics regime

Modeling a dense aggregate with millions of irregular particles in the geometric optics regime is a computationally intensive task. The problem is that, if there is only low absorption present, the rays can keep splitting without ever escaping the medium (see Sec. 3.2). For that reason, the possibility of using the diffuse scattering to approximate the multiple scattering in the geometric optics regime was studied in Paper VI.

In order to approximate the geometric optics, the pure diffuse model needs to be investigated. First, the diffuse model lacks any surface features because it assumes the medium to be statistical, thus lacking, e.g., shadowing (see Fig. 3.2). Shadowing produces distinctive scattering characteristics, and thus omitting it is a severe over-simplification. For example, the shadowing was earlier considered to be the main cause of the opposition brightening of the lunar regolith (Hapke, 1963). Hence, there has been research on how to add shadowing by including surface roughness to the diffuse model (Irvine, 1966; Lumme et al., 1990; Peltoniemi and Lumme, 1992). In Paper VI, the accurate presentation of the surface, and thus shadowing effects, is included by generating a mantle made of the properly characterized particles that is placed on top of the diffusely scattering medium (hybrid model, see Fig. 4.1). It is simple but more compute-intensive than the pure diffuse approach or some function approximating the surface characteristics.

The other simplification in the diffuse model is the extinction mean free path distance, which is used to determine the distance between the diffuse scattering events. The classical extinction mean free path length contains information about the volume fraction and the extinction cross-section but nothing about specific scattering properties or the size difference between the particles. The exponential attenuation model can be derived alongside the RT theory, so it works for small scatterers in sparse media but not when the particles are in close contact and large. In order to improve the model, in Paper VI, the exponential attenuation model is replaced

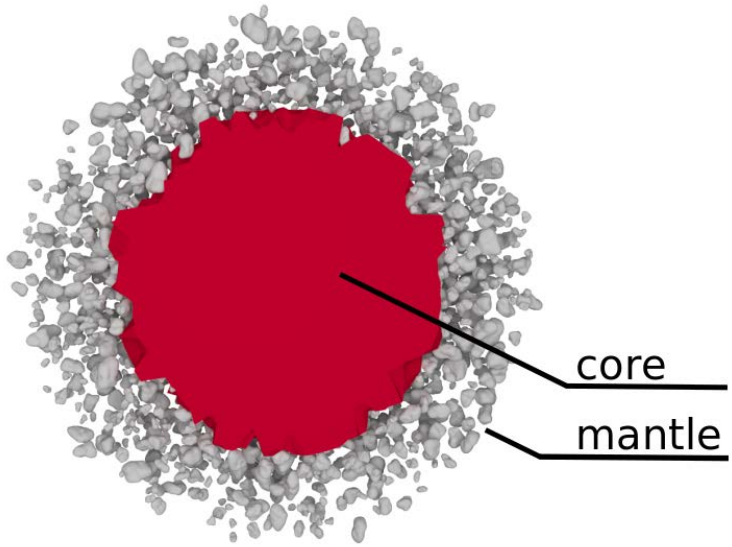

Figure 4.1: A cross section of the hybrid model.

with an exponential distance distribution that is simulated numerically before the actual computation. The distribution is gathered by running a mock run with the accurately discretized medium that tracks the lengths between the first refraction, reflection, or absorption points (see Fig. 4.2). From this distribution, distances for the ray inside the diffuse medium can be drawn during the actual run, which removes the need for an approximation with the attenuation.

In order to study the methods, in Paper VI the light-scattering properties of a spherical medium of kR=2000, made of GRS particles with the refractive index m=1.6+i0.0001 that follow a power-law size-distribution was simulated. We used the diffuse method, the hybrid model with the extinction distance distribution, and the geometric-optics-only method, in which no approximations outside the generalized Snel's law and Fresnel matrices were used. The geometric optics model was considered as the ground-truth. The comparison showed that the hybrid model with the extinction distance distribution is capable of correcting most issues the diffuse model has.

This new hybrid model is relatively straightforward because it does not need any approximations such as the Percus-Yevick or shadowing functions to be developed. The mantle can be made from the same particle geometries that are needed to compute the diffuse scattering properties, and the extinction distribution is acquired

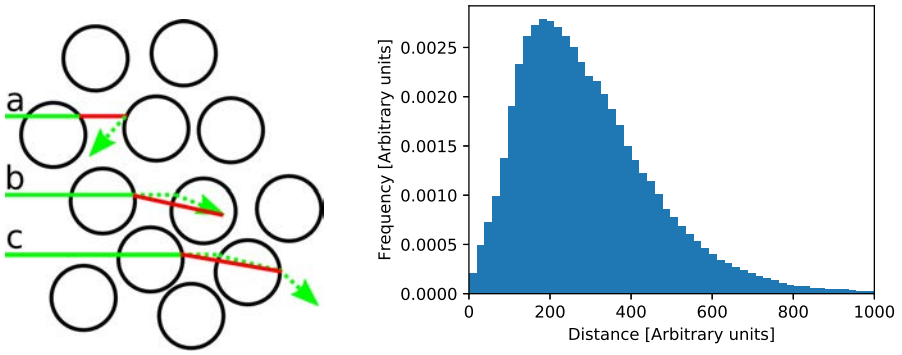

Figure 4.2: Extinction mean free path distribution is collected by recording the lengths from the first reflection (a), absorption (b), or refraction points (c).

numerically from the simulation (see Fig. 4.2). Although the results were promising, the model can still be improved further. The distance distribution considered the first particle that the ray intersected, but it could be easily extended to consider the second and third particles. This way, the distance to the second-order or third-order diffuse scattering is computed from different distributions, making the presentation of the extinction distances more accurate because the polarization states after the first scattering are different from the initial polarization state. The changed polarization state affects the intensity of the refracted and reflected rays, meaning that the extinction distance distribution is not the same after each scattering from a particle.

4.3 Modeling real samples

Demonstrating that the methods work by validating them against the measurements of real samples is not an easy task. Modeling the light-scattering characteristics depends on numerous parameters from collective to single-particle properties, meaning that there are many parameters to test. The problem is that two sets of parameters can give the same normalized phase functions, which hinders the interpretation of the measured data. Therefore, the methods should always be validated first against well-controlled samples before using for characterizations, even if they seem to compare well against the established numerical methods.

In Muinonen et al. (2019), an aggregate of $\varnothing$=0.5 µm made of densely packed equisized spherical silicate particles was created (Weidling et al., 2012; Blum et al., 2014) and the light-scattering properties were measured in the laboratory by the non-destructive controlled single-particle light scattering measurement that uses an

acoustic levitator (Maconi et al., 2018). The sample was then modeled numerically with the simplified R^2T^2 methodology by using SIRIS with the added coherent effects as in Markkanen et al. (2018). Different underlying size distributions of the particles inside the volume elements were tested, which revealed that the particles inside the aggregate were not equisized anymore — better results were obtained by using a distribution with smaller particles. The normalized phase functions turned out to be insensitive to the size distribution. It was is the depolarization and the degree of linear polarization that could be used to discriminate among the underlying size distributions. The simulations hinted that there are multiple smaller particles, which indicates that the particles were fractured due to the applied pressure when the aggregate was made from the silicate powder, meaning that the size distribution of the particles was not well-controlled. The sample was not imaged with the scanning electron microscope (SEM) because that would have destroyed the sample.

In Paper VII, another sample was modeled to test the applicability of the R^2T^2. The sample was one of the agglomerates created for the study that characterized the light-scattering properties by using the PROGRA^2 instrument (Hadamcik et al., 2007; Levasseur-Regourd et al., 2015). In Paper VII, an agglomerate made of equisized silica spheres was modeled by following Markkanen et al. (2018) and starting with the parameters derived in the experimental paper (Hadamcik et al., 2007). The study revealed that the R^2T^2 is capable of simulating the phase function, but there are discrepancies in the degree of polarization, meaning that the R^2T^2 should be developed further. Still, the results were promising, and the R^2T^2 could be applied in more complicated characterization. The study ended up in a similar conclusion to that in Muinonen et al. (2019) that the degree of linear polarization is beneficial for the physical characterization because all the characteristics (size distribution) are not easily derived from the normalized phase function.

5 Summary of the publications

This thesis consists of one refereed conference proceedings article and six refereed journal publications.

- **Paper I:** Väisänen T., Penttilä A., Markkanen J., Muinonen K., (2016), Validation of radiative transfer and coherent backscattering for discrete random media, *2016 URSI International Symposium on Electromagnetic Theory (EMTS),* 396–399.
- **Paper II:** Muinonen K., Markkanen J., Väisänen T., Peltoniemi J. I., Penttilä A., (2017), Multiple scattering in discrete random media using first-order incoherent interactions, *Radio Science*, 52:1419–1431.
- **Paper III:** Muinonen K., Markkanen J., Väisänen T., Peltoniemi J., Penttilä A., (2018), Multiple scattering of light in discrete random media using incoherent interactions, *Optics Letters*, 43:683–686.
- **Paper IV:** Markkanen J., Väisänen T., Penttilä A., Muinonen K., (2018), Scattering and absorption in dense discrete random media of irregular particles, *Optics Letters*, 43:2925–2928.
- **Paper V:** Väisänen T., Markkanen J., Penttilä A., Muinonen K., (2019), Radiative transfer with reciprocal transactions: Numerical method and its implementation, *PLOS ONE*. 14(1).
- **Paper VI:** Väisänen T., Martikainen J., Muinonen K., (2020), Scattering of light by dense particulate media in the geometric optics regime, *Journal of Quantitative Spectroscopy and Radiative Transfer*, 241.
- **Paper VII:** Väisänen T., Markkanen J., Hadamcik E., Renard J.-B., Lasue J., Levasseur-Regourd A.C., Blum J., and Muinonen K., (2020), Scattering of light by a large, densely-packed agglomerate of small silica spheres, *Optics Letters*, 45:1679–1682.

5.1 Paper I

We studied the applicability of the RT-CB by comparing it to the MSTM. The spherical discrete random medium composed of spherical particles with varying volume fraction were studied, while the number of particles was kept constant. The light-scattering properties were simulated using the MSTM and the RT-CB, and then compared. The conclusion was that the RT-CB is applicable to the small medium (radius $kR \approx 86$, particle radius $ka=2$, refractive index $m=1.31$), where the volume fraction v is below 0.1. The study was a continuation of the study by Muinonen et al. (2012).

For the paper, the author computed the RT-CB results and wrote the manuscript. The author programmed the open-source and modernized version of the RT-CB software that was based on the older RT-CB software programmed originally by K. Muinonen. The modernized RT-CB worked as a framework for the prototype $\mathrm{R^2T^2}$, which was presented in Muinonen et al. (2016). The MSTM results were computed and normalized by A. Penttilä and J. Markkanen.

5.2 Paper II

The derivation of the theory behind the first-order incoherent volume element was presented. The method was validated by computing the light-scattering properties of the first-order incoherent volume elements, which were then used as input for the RT-CB (the first-order $\mathrm{R^2T^2}$) for various particulate media (ice $m=1.31$ and silicate $m=1.5$, $ka=2$ and $ka=1.76$, $kR=50$, v from 0.03 to 0.25). These $\mathrm{R^2T^2}$ results were then compared to the results computed with the FaSTMM. The results matched in a satisfactory way.

The author has been part of the $\mathrm{R^2T^2}$ development group (all the co-authors) since the beginning. He has been responsible for testing the ideas that were devised during weekly discussions. For the paper, the author tested various incoherent volume elements with different packing algorithms and commented on the manuscript.

5.3 Paper III

The $\mathrm{R^2T^2}$ was presented in its current form and was shown to extend the applicability of the RT by simulating light scattering from dense random spherical media ($kR=100$, $ka=2$, $m=1.31$, $v=0.125$, and $v=0.25$). The letter introduced the proper creation of the incoherent volume element and validated the method by comparing it to the

FaSTMM. Moreover, the light scattering characteristics of large media (kR=10000, v=0.125, and v=0.25) that are far out of reach of the exact methods were computed to show the capabilities of the R^2T^2.

The author developed the volume element generator and the R^2T^2 with J. Markkanen, who was responsible for the T-matrix related functions and the software that computed the incoherent light-scattering properties of the volume elements. For the paper, the author commented on the manuscript, computed the R^2T^2 results, and provided the data related to the R^2T^2 software.

5.4 Paper IV

The paper is a continuation of Paper III. The R^2T^2 is applied to the particulate medium composed of irregular particles. The R^2T^2 uses the T-matrix formalism, which makes it possible to incorporate arbitrary particles as scatterers. The incoherent volume elements were generated with the volume integral equation solver JVIE. The R^2T^2 was validated against the JVIE method by simulating particulate media of size kR=60 with volume fractions v=0.125 and v=0.25. Also, light-scattering properties of a discrete random medium consisting of spherical particles were compared to the medium with irregular particles: Significant differences were revealed between them. Finally, another large $kR \approx 1.2 \times 10^{13}$ medium with irregular particles was simulated with the R^2T^2 to show its capabilities.

The author took part in the development of the R^2T^2 software and commented on the manuscript.

5.5 Paper V

The algorithm and details of the R^2T^2 are described. The decisions affecting the generation of the incoherent volume element are discussed, and the validation is extended from Paper III by using various refractive indices. The method is validated by simulating different spherical particulate media composed of spherical particles and comparing the results to the results obtained with the FaSTMM. The comparison is consistent with Paper III, and the R^2T^2 is shown to be capable of simulating diffuse scattering in the dense medium.

The author was responsible for writing the manuscript, excluding the T-matrix theory part, which was written by J. Markkanen. The author computed all the R^2T^2 and the incoherent volume element related data.

5.6 Paper VI

In Paper VI, the applicability of the RT to dense particulate media in the geometric optics regime is studied. The new SIRIS is implemented and is capable of computing light scattering by particulate medium consisting of different materials. Alongside the comparison, we present a hybrid diffuse geometric optics method that uses the extinction distance distribution instead of the single extinction mean free path. The pure diffuse model and the hybrid model are compared to the "ground truth", in which only the generalized Snel's law and Fresnel matrices are used. All the scattering elements show that the hybrid model with the extinction distance distribution is on par with the "ground truth."

The author planned the research in cooperation with K. Muinonen. The author computed all the results and wrote the manuscript. For the paper, the author independently revised the SIRIS framework that was based on the older SIRIS by K. Muinonen, H. Lindqvist, and J. Martikainen. The author also devised and implemented the multiparticle mesh generator and the hybrid model. J. Martikainen helped by checking the extinction mean free paths.

5.7 Paper VII

The simplified R^2T^2 was used to model a levitating sample that showed that the physical characterization disagreed with the given parameters (Muinonen et al., 2019). In Paper VII, the R^2T^2 is used to model another analog sample made of closely equisized spherical silica spheres, with well-controlled physical properties. We also studied the effects of the effective medium approximation and how the geometry of the diffusely scattering medium affects the results. We managed to recreate the phase function with the given physical parameters, and by tweaking them, also the degree of linear polarization.

The author planned the research in cooperation with K. Muinonen. The author was responsible for writing the manuscript and computing the results with the methods discussed in this thesis. J. Blum provided the included SEM image, whereas the measurements were provided by the co-authors from France.

5.8 Publications not included in the thesis

In addition to Papers I–VII, the author has contributed to the following papers

- Muinonen K., Markkanen J., Penttilä A., Väisänen T., Peltoniemi J., (2016), Multiple scattering by dense random media: Numerical solution, *2016 URSI International Symposium on Electromagnetic Theory (EMTS)*, 400–403.
- Markkanen J., Agarwal J., Väisänen T., Penttilä A., Muinonen K., (2018), Interpretation of the phase functions measured by the OSIRIS instrument for comet 67P/Churyumov–Gerasimenko, *The Astrophysical Journal*, 868(1).
- Muinonen K., Väisänen T., Martikainen J., Markkanen J., Penttilä A., Gritsevich M., Peltoniemi J., Blum J., Herranen J., Videen G., Maconi G., Helander P., Salmi A., Kassamakov I., Haeggström E., (2019), Scattering and absorption of light in planetary regoliths, *Journal of Visualized Experiments*, 149.

6 Concluding remarks

The thesis is a part of a venture that thrives toward finding a solution to a long-term open problem of how to simulate the multiple scattering of light by dense discrete random media, such as a planetary regolith. The main topic of the thesis is the use of the diffuse scattering as a tool to approximate the light scattering in particulate media. In Papers I–V, the focus is on the resonance regime, whereas Paper VI focuses on the geometric optics regime. Finally, the software and findings in these papers are used to model a real sample in Paper VII.

The idea for the R^2T^2 was conceptualized when the RT-CB was shown to work for a small sparse medium with modest numbers of particles, despite the requirement of the RT theory that the particle count must be very large. In Paper II, the R^2T^2 was created based on the previous works with the incoherent electric fields, and new simulations that successfully modeled the dense discrete random medium using the incoherent first-order volume elements. In Papers III–V, the R^2T^2 was described in detail with validations where the light-scattering properties of different discrete random media were computed with the R^2T^2 and the exact methods. Finally, the R^2T^2 was validated by simulating a real sample that had well-controlled physical properties using the software developed for Paper VI, in which diffuse scattering in the geometric optics regime was studied. The R^2T^2 was able to simulate the phase function of the real sample well, but it was the degree of linear polarization that revealed the discrepancies in the simulation. By adjusting the given physical properties, a better match with the measurements was achieved. The R^2T^2 in its current state was shown to simulate the light scattering properties of the agglomerate well. The conclusion emphasizes the previous conclusions that the degree of linear polarization contains information that facilitates physical characterization.

The motivation for the thesis is to create light-scattering tools that could be used to characterize the physical features of the remotely observed objects. If done correctly and with foundation based on physics, the method makes it possible to model arbitrary regoliths computationally. This would speed up the physical characterization of the regolith on the Earth, asteroids, the Moon, or any particulate object, and make it possible to simulate regoliths with well-controlled features that

are harder to create in the laboratory. We conclude that the R^2T^2 should be studied and developed further, in order to establish a robust method that could be used for the physical characterization work in the future. In the current state, the R^2T^2 has been shown to work relatively well, which is backed up with the computational (Papers III–V) and experimental validations (Paper VII). Still, there are issues that need to be addressed.

The first issue is the size of the volume element, which is likely to be related to the exponential attenuation from the RT theory. In Paper VI, the attenuation model was replaced with the extinction distance distribution, and something similar could be implemented into the R^2T^2, although it is not as easy as with the RT. In order to replace exponential attenuation, the internal field of the medium should be studied. This could also be used to improve the selection of the scattering direction of the ray, which in Papers III–V is based on the scattered far fields around the volume element.

The second issue is the coherent field effects that are not included in the R^2T^2, although they were added to the simplified version of the R^2T^2 as a geometric optics approximation. The problem is that the coherent effects are currently computed from the small volume elements, although the coherent effects are due to the larger features of the medium, such as the local surface. There is also a related problem of how to add the CB properly to the R^2T^2 with the added coherent effects. All issues would be easier to deal with if a thorough theoretical derivation of the R^2T^2 would be established, the same way as the RT theory has been established from the Maxwell equations.

What comes to the development of SIRIS, the physics parts could be rewritten in order to add CB capabilities for diffuse computations, which would benefit the current user base of the SIRIS who use it as a physical characterization tool. Increased computational performance can be achieved with the implementation of a specialized ray-tracing engine, which is important because the physical characterization requires ensemble-averaging and simulation of multiple wavelengths with different physical parameters. The extinction distance distributions studied in Paper VI could be expanded to consider the second and third particle scattering distances, making the distances between diffuse scatterings more accurate.

The ongoing space missions provide future applications for the R^2T^2. The Gaia mission produces visible spectra for the asteroid classification purposes, whereas BepiColombo will measure the light-scattering properties of the regolith of Mercury. The spectra provided by these missions can be analyzed with the R^2T^2, which can help to characterize the underlying physical properties of the regolith.

Bibliography

Aster, R., Borchers, B., and Thurber, C. (2011). *Parameter estimation and inverse problems*. International Geophysics. Elsevier Science.

Babenko, V., Astafyeva, L., Kuzmin, V., and Kuz'min, V. (2003). *Electromagnetic scattering in disperse media: Inhomogeneous and anisotropic particles*. Environmental Sciences. Springer.

Belton, M. J. S., Veverka, J., Thomas, P., Helfenstein, P., Simonelli, D., Chapman, C., Davies, M. E., Greeley, R., Greenberg, R., Head, J., Murchie, S., Klaasen, K., Johnson, T. V., McEwen, A., Morrison, D., Neukum, G., Fanale, F., Anger, C., Carr, M., and Pilcher, C. (1992). Galileo encounter with 951 Gaspra: First pictures of an asteroid. *Science*, 257(5077):1647–1652.

Blum, J., Beitz, E., Bukhari, M., Gundlach, B., Hagemann, J.-H., Heißelmann, D., Kothe, S., Schräpler, R., von Borstel, I., and Weidling, R. (2014). Laboratory drop towers for the experimental simulation of dust-aggregate collisions in the early solar system. *Journal of Visualized Experiments*.

Bohren, C. F. and Huffman, D. R. (1983). *Absorption and scattering of light by small particles*. New York: Wiley, 1983.

Bruning, J. and Lo, Y. (1971a). Multiple scattering of EM waves by spheres I. Multipole expansion and ray-optical solutions. *IEEE Transactions on Antennas and Propagation*, 19:378–390.

Bruning, J. and Lo, Y. (1971b). Multiple scattering of EM waves by spheres II. Numerical and experimental results. *IEEE Transactions on Antennas and Propagation*, 19:391–400.

Bus, S. J. and Binzel, R. P. (2002). Phase II of the small main-belt asteroid spectroscopic survey. A feature-based taxonomy. *Icarus*, 158:146–177.

Chandrasekhar, S. (1960). *Radiative transfer*. Dover Books on Intermediate and Advanced Mathematics. Dover Publications.

Chang, P. C., Walker, J., and Hopcraft, K. (2005). Ray tracing in absorbing media. *Journal of Quantitative Spectroscopy and Radiative Transfer*, 96(3):327 – 341.

Chew, W. C., Jiang, L. J., Sun, S., Sha, W. E. I., Dai, Q. I., Fallahpour, M., and Wu, Y. M. (2016). Numerical modeling in antenna engineering. In Chen, Z. N., editor, *Handbook of Antenna Technologies*, pages 1–71. Springer Singapore, Singapore.

Chowdhary, J., Zhai, P.-W., Boss, E., Dierssen, H., Frouin, R., Ibrahim, A., Lee, Z., Remer, L. A., Twardowski, M., Xu, F., Zhang, X., Ottaviani, M., Espinosa, W. R., and Ramon, D. (2019). Modeling atmosphere-ocean radiative transfer: A PACE mission perspective. *Frontiers in Earth Science*, 7:100.

Clark, B. E., Hapke, B., Pieters, C., and Britt, D. (2002). Asteroid space weathering and regolith evolution. In Bottke, Jr., W. F., Cellino, A., Paolicchi, P., and Binzel, R. P., editors, *Asteroids III*, pages 585–599. University of Arizona Press, Tucson.

CLASS (2019). Planetary simulant database. `https://sciences.ucf.edu/class/planetary-simulant-database/`. Accessed: 2019-11-05.

Cloutis, E. A., Binzel, R. P., and Gaffey, M. J. (2014). Establishing asteroid–meteorite links. *Elements*, 10(1):25–30.

Cohen-Tannoudji, C., Dupont-Roc, J., and Grynberg, G. (1989). *Photons and Atoms: Introduction to Quantum Electrodynamics*. Wiley.

Cottini, V., Nixon, C., Jennings, D., de Kok, R., Teanby, N., Irwin, P., and Flasar, F. (2012). Spatial and temporal variations in Titan's surface temperatures from Cassini CIRS observations. *Planetary and Space Science*, 60(1):62 – 71.

Cruikshank, D. P., Ore, C. M. D., Roush, T. L., Geballe, T. R., Owen, T. C., de Bergh, C., Cash, M. D., and Hartmann, W. K. (2001). Constraints on the composition of Trojan asteroid 624 Hektor. *Icarus*, 153(2):348 – 360.

de Lange Kristiansen, K., Wouterse, A., and Philipse, A. (2005). Simulation of random packing of binary sphere mixtures by mechanical contraction. *Physica A: Statistical Mechanics and its Applications*, 358(2):249 – 262.

DeMeo, F. E., Binzel, R. P., Slivan, S. M., and Bus, S. J. (2009). An extension of the Bus asteroid taxonomy into the near-infrared. *Icarus*, 202:160–180.

Dupertuis, M. A., Proctor, M., and Acklin, B. (1994a). Generalization of complex Snell–Descartes and Fresnel laws. *Journal of the Optical Society of America A*, 11(3):1159–1166.

Dupertuis, M. A., Acklin, B., and Proctor, M. (1994b). Generalized energy balance and reciprocity relations for thin-film optics. *Journal of the Optical Society of America A*, 11(3):1167–1174.

Egel, A., Pattelli, L., Mazzamuto, G., Wiersma, D. S., and Lemmer, U. (2017). Celes: Cuda-accelerated simulation of electromagnetic scattering by large ensembles of spheres. *Journal of Quantitative Spectroscopy and Radiative Transfer*, 199:103 – 110.

Epstein, P. S. (1930). Geometrical optics in absorbing media. *Proceedings of the National Academy of Sciences*, 16(1):37–45.

Foldy, L. L. (1945). The multiple scattering of waves. I. General theory of isotropic scattering by randomly distributed scatterers. *Physical Review*, 67:107–119.

Gehrels, T., Coffeen, T., and Owings, D. (1964). Wavelength dependance of polarization. III. The lunar surface. *The Astronomical Journal*, 69:826.

Griffiths, D. J. (2013). *Introduction to electrodynamics; 4th ed.* Pearson, Boston, MA. Re-published by Cambridge University Press in 2017.

Grynko, Y., Shkuratov, Y., and Förstner, J. (2016). Light scattering by irregular particles much larger than the wavelength with wavelength-scale surface roughness. *Optics Letters*, 41(15):3491–3494.

Hadamcik, E., Renard, J.-B., Lasue, J., Levasseur-Regourd, A., Blum, J., and Schraepler, R. (2007). Light scattering by low-density agglomerates of micron-sized grains with the PROGRA2 experiment. *Journal of Quantitative Spectroscopy and Radiative Transfer*, 106(1):74 – 89.

Hadamcik, E., Levasseur-Regourd, A., Renard, J.-B., Lasue, J., and Sen, A. (2011). Polarimetric observations and laboratory simulations of asteroidal surfaces: The case of 21 Lutetia. *Journal of Quantitative Spectroscopy and Radiative Transfer*, 112(11):1881 – 1890.

Hapke, B. (1981). Bidirectional reflectance spectroscopy: 1. theory. *Journal of Geophysical Research: Solid Earth*, 86(B4):3039–3054.

Hapke, B. (2008). Bidirectional reflectance spectroscopy: 6. effects of porosity. *Icarus*, 195(2):918 – 926.

Hapke, B. (2013). Comment on "A critical assessment of the Hapke photometric model" by Y. Shkuratov et al. *Journal of Quantitative Spectroscopy and Radiative Transfer*, 116:184–190.

Hapke, B. W. (1963). A theoretical photometric function for the lunar surface. *Journal of Geophysical Research (1896-1977)*, 68(15):4571–4586.

Hapke, B. W., Nelson, R. M., and Smythe, W. D. (1993). The opposition effect of the moon: The contribution of coherent backscatter. *Science*, 260(5107):509–511.

He, D., Ekere, N., and Cai, L. (2000). Computer simulation of the random packing of unequal particles. *Physical review. E, Statistical physics, plasmas, fluids, and related interdisciplinary topics*, 60:7098–104.

Hovenier, J. W. and van der Mee, C. V. M. (1988). Scattering of polarized light - Properties of the elements of the phase matrix. *Astronomy & Astrophysics*, 196(1-2):287–295.

Irvine, W. M. (1966). The shadowing effect in diffuse reflection. *Journal of Geophysical Research (1896-1977)*, 71(12):2931–2937.

Ishimaru, A. and Kuga, Y. (1982). Attenuation constant of a coherent field in a dense distribution of particles. *J. Opt. Soc. Am. (1917–1983)*, 72:1317.

Ito, G., Arnold, J. A., and Glotch, T. D. (2017). T-matrix and radiative transfer hybrid models for densely packed particulates at mid-infrared wavelengths. *Journal of Geophysical Research: Planets*, 122(5):822–838.

Jackson, J. D. (1999). *Classical electrodynamics*. Wiley, New York, NY, 3rd ed. edition.

Kaasalainen, M. and Torppa, J. (2001). Optimization methods for asteroid lightcurve inversion: I. shape determination. *Icarus*, 153(1):24 – 36.

Kohout, T., Čuda, J., Filip, J., Britt, D., Bradley, T., Tuček, J., Skála, R., Kletetschka, G., Kašlík, J., Malina, O., Šišková, K., and Zbořil, R. (2014). Space weathering simulations through controlled growth of iron nanoparticles on olivine. *Icarus*, 237:75 – 83.

Kolokolova, L., Hanner, M. S., Levasseur-Regourd, A.-C., and Gustafson, B. Å. S. (2004). Physical properties of cometary dust from light scattering and thermal emission. In Festou, M. C., Keller, H. U., and Weaver, H. A., editors, *Comets II*, pages 577–604. University of Arizona Press, Tucson.

Kolokolova, L., Petrova, E., and Kimura, H. (2011). Effects of interaction of electromagnetic waves in complex particles. In Zhurbenko, V., editor, *Electromagnetic Waves*, chapter 9. IntechOpen, Rijeka.

Lampe, B., Holliger, K., and Green, A. G. (2003). A finite-difference time-domain simulation tool for ground-penetrating radar antennas. *GEOPHYSICS*, 68(3):971–987.

Lax, M. (1951). Multiple scattering of waves. *Reviews of Modern Physics*, 23:287–310.

Lax, M. (1952). Multiple scattering of waves. II. The effective field in dense systems. *Physical Review*, 85:621–629.

Levasseur-Regourd, A., Renard, J.-B., Shkuratov, Y., and Hadamcik, E. (2015). Laboratory studies. In Kolokolova, L., Hough, J., and Levasseur-Regourd, A., editors, *Polarimetry of stars and planetary systems*, pages 62–80. Cambridge University Press.

Lindqvist, H., Martikainen, J., Räbinä, J., Penttilä, A., and Muinonen, K. (2018). Ray optics for absorbing particles with application to ice crystals at near-infrared wavelengths. *Journal of Quantitative Spectroscopy and Radiative Transfer*, 217:329 – 337.

Lumme, K. and Bowell, E. (1981). Radiative transfer in the surfaces of atmosphereless bodies. I. Theory. *Astronomical Journal*, 86:1694–1721.

Lumme, K., Peltoniemi, J. I., and Irvine, W. M. (1990). Diffuse reflection from a stochastically bounded, semi-infinite medium. *Transport Theory and Statistical Physics*, 19(3-5):317–332. PMID: 11539101.

Mackowski, D. and Mishchenko, M. (2011). A multiple sphere T-matrix Fortran code for use on parallel computer clusters. *Journal of Quantitative Spectroscopy and Radiative Transfer*, 112(13):2182 – 2192.

Maconi, G., Penttilä, A., Kassamakov, I., Gritsevich, M., Helander, P., Puranen, T., Salmi, A., Hæggström, E., and Muinonen, K. (2018). Non-destructive controlled

single-particle light scattering measurement. *Journal of Quantitative Spectroscopy and Radiative Transfer*, 204:159 – 164.

Mallama, A., Wang, D., and Howard, R. A. (2002). Photometry of Mercury from SOHO/LASCO and Earth: The phase function from 2 to 170°. *Icarus*, 155(2):253 – 264.

Markkanen, J., Yla-Oijala, P., and Sihvola, A. (2012). Discretization of volume integral equation formulations for extremely anisotropic materials. *IEEE Transactions on Antennas and Propagation*, 60(11):5195–5202.

Markkanen, J. and Yuffa, A. J. (2017). Fast superposition T-matrix solution for clusters with arbitrarily-shaped constituent particles. *Journal of Quantitative Spectroscopy and Radiative Transfer*, 189:181 – 188.

Markkanen, J., Agarwal, J., Väisänen, T., Penttilä, A., and Muinonen, K. (2018). Interpretation of the phase functions measured by the OSIRIS instrument for comet 67P/Churyumov–Gerasimenko. *The Astrophysical Journal*, 868(1):L16.

Martikainen, J., Penttilä, A., Gritsevich, M., Lindqvist, H., and Muinonen, K. (2018). Spectral modeling of meteorites at UV-vis-NIR wavelengths. *Journal of Quantitative Spectroscopy and Radiative Transfer*, 204:144 – 151.

Martikainen, J., Penttilä, A., Gritsevich, M., Videen, G., and Muinonen, K. (2019). Absolute spectral modelling of asteroid (4) Vesta. *Monthly Notices of the Royal Astronomical Society*, 483(2):1952–1956.

Mishchenko, M., , Travis, L., and Lacis, A. (2006). *Multiple scattering of light by particles: Radiative transfer and coherent backscattering*. Cambridge University Press.

Muinonen, K. (1990). *Light scattering by inhomogeneous media: backward enhancement and reversal of linear polarization*. Observatory and Astrophysics Laboratory, University of Helsinki, Finland.

Muinonen, K., Nousiainen, T., Fast, P., Lumme, K., and Peltoniemi, J. (1996). Light scattering by Gaussian random particles: Ray optics approximation. *Journal of Quantitative Spectroscopy and Radiative Transfer*, 55(5):577 – 601.

Muinonen, K. (2004). Coherent backscattering of light by complex random media of spherical scatterers: numerical solution. *Waves in Random Media*, 14(3):365–388.

Muinonen, K., Nousiainen, T., Lindqvist, H., Muñoz, O., and Videen, G. (2009). Light scattering by Gaussian particles with internal inclusions and roughened surfaces using ray optics. *Journal of Quantitative Spectroscopy and Radiative Transfer*, 110(14):1628 – 1639.

Muinonen, K., Parviainen, H., Näränen, J., Josset, J.-L., Beauvivre, S., and Pinet, P. (2011). Lunar surface properties with SMART-1 AMIE. *Astronomy & Astrophysics*, 531.

Muinonen, K., Mishchenko, M. I., Dlugach, J. M., Zubko, E., Penttilä, A., and Videen, G. (2012). Coherent backscattering verified numerically for a finite volume of spherical particles. *Astrophysical Journal*, 760:118.

Muinonen, K., Markkanen, J., Penttilä, A., Väisänen, T., and Peltoniemi, J. (2016). Multiple scattering by dense random media: Numerical solution. In *2016 URSI International Symposium on Electromagnetic Theory (EMTS)*, pages 400–403.

Muinonen, K., Väisänen, T., Martikainen, J., Markkanen, J., Penttilä, A., Gritsevich, M., Peltoniemi, J., Blum, J., Herranen, J., Videen, G., Maconi, G., Helander, P., Salmi, A., Kassamakov, I., and Haeggström, E. (2019). Scattering and absorption of light in planetary regoliths. *Journal of Visualized Experiments*, 149(e59607).

Nieminen, T., Rubinsztein-Dunlop, H., and Heckenberg, N. (2003). Calculation of the T-matrix: General considerations and application of the point-matching method. *Journal of Quantitative Spectroscopy and Radiative Transfer*, 79-80:1019 – 1029.

Peltoniemi, J. I., Lumme, K., Muinonen, K., and Irvine, W. M. (1989). Scattering of light by stochastically rough particles. *Applied Optics*, 28(19):4088–4095.

Peltoniemi, J. I. and Lumme, K. (1992). Light scattering by closely packed particulate media. *Journal of the Optical Society of America A*, 9(8):1320–1326.

Peterson, B. and Ström, S. (1973). T-matrix for electromagnetic scattering from an arbitrary number of scatterers and representations of E(3). *Physical Review D*, 8:3661–3678.

Pfalzner, S., Davies, M. B., Gounelle, M., Johansen, A., Münker, C., Lacerda, P., Zwart, S. P., Testi, L., Trieloff, M., and Veras, D. (2015). The formation of the solar system. *Physica Scripta*, 90(6):068001.

Pieters, C. M. and Noble, S. K. (2016). Space weathering on airless bodies. *Journal of Geophysical Research: Planets*, 121(10):1865–1884.

Ramezanpour, B. and Mackowski, D. W. (2019). Direct prediction of bidirectional reflectance by dense particulate deposits. *Journal of Quantitative Spectroscopy and Radiative Transfer*, 224:537 – 549.

Russell, C. and Raymond, C. (2011). The Dawn mission to Vesta and Ceres. *Space Science Reviews*, 163.

Räbinä, J., Mönkölä, S., and Rossi, T. (2015). Efficient time integration of Maxwell's equations with generalized finite differences. *SIAM Journal on Scientific Computing*, 37(6):B834–B854.

Seeliger, H. (1887). *Zur Theorie der Beleuchtung der großen Planeten, insbesondere des Saturn.* Abhandlungen d. math.-phys. Cl. d. kgl. bayer. Akad. d. Wiss. 16, 2. Verlag d. K. Akad.

Shepard, M. K. and Helfenstein, P. (2007). A test of the Hapke photometric model. *Journal of Geophysical Research: Planets*, 112(E3).

Shkuratov, I. G. (1988). A diffraction mechanism for the formation of the opposition effect of the brightness of surfaces having a complex structure. *Kinematika i Fizika Nebesnykh Tel*, 4:33–39.

Shkuratov, Y., Kaydash, V., Korokhin, V., Velikodsky, Y., Petrov, D., Zubko, E., Stankevich, D., and Videen, G. (2012). A critical assessment of the Hapke photometric model. *Journal of Quantitative Spectroscopy and Radiative Transfer*, 113(18):2431 – 2456.

Shkuratov, Y., Kaydash, V., Korokhin, V., Velikodsky, Y., Petrov, D., Zubko, E., Stankevich, D., and Videen, G. (2013). Response to the comment by B. Hapke on "A critical assessment of the Hapke photometric model". *Journal of Quantitative Spectroscopy and Radiative Transfer*, 116:191 – 195.

Simonelli, D. P., Veverka, J., Thomas, P. C., Helfenstein, P., Carcich, B. T., and Belton, M. J. (1996). Ida lightcurves: Consistency with Galileo shape and photometric models. *Icarus*, 120(1):38 – 47.

Stankevich, D. G. and Shkuratov, Y. G. (2002). Multiple scattering of light in regolith-like media: Geometric optics approximation. *Solar System Research*, 36(5):409–416.

Sun, Z., Lv, Y., and Lu, S. (2015). An assessment of the bidirectional reflectance models basing on laboratory experiment of natural particulate surfaces. *Journal of Quantitative Spectroscopy and Radiative Transfer*, 163:102 – 119.

Tang, H., Wang, S., and Li, X. (2012). Simulation of nanophase iron production in lunar space weathering. *Planetary and Space Science*, 60(1):322 – 327.

Tholen, D. J. (1989). Asteroid taxonomic classifications. In Binzel, R. P., Gehrels, T., and Matthews, M. S., editors, *Asteroids II*, pages 1139–1150.

Tsang, L., Kong, J., and Shin, R. (1985). *Theory of microwave remote sensing*. John Wiley & Sons, Incorporated.

Tsang, L. and Ishimaru, A. (1987). Radiative wave equations for vector electromagnetic propagation in dense nontenuous media. *Journal of Electromagnetic Waves and Applications*, 1(1):59–72.

Tsang, L., Mandt, C. E., and Ding, K. H. (1992). Monte Carlo simulations of the extinction rate of dense media with randomly distributed dielectric spheres based on solution of Maxwell's equations. *Optics Letters*, 17(5):314–316.

Tsang, L., Chen, C.-T., Chang, A. T. C., Guo, J., and Ding, K.-H. (2000). Dense media radiative transfer theory based on quasicrystalline approximation with applications to passive microwave remote sensing of snow. *Radio Science*, 35(3):731–749.

Tsang, L., Kong, J., Ding, K., and Ao, O. (2001). *Scattering of electromagnetic waves, numerical simulations*, volume 2. Wiley.

Tsuchiyama, A., Uesugi, M., Matsushima, T., Michikami, T., Kadono, T., Nakamura, T., Uesugi, K., Nakano, T., Sandford, S. A., Noguchi, R., Matsumoto, T., Matsuno, J., Nagano, T., Imai, Y., Takeuchi, A., Suzuki, Y., Ogami, T., Katagiri, J., Ebihara, M., Ireland, T. R., Kitajima, F., Nagao, K., Naraoka, H., Noguchi, T., Okazaki, R., Yurimoto, H., Zolensky, M. E., Mukai, T., Abe, M., Yada, T., Fujimura, A., Yoshikawa, M., and Kawaguchi, J. (2011). Three-dimensional structure of Hayabusa samples: Origin and evolution of Itokawa regolith. *Science*, 333(6046):1125–1128.

Twersky, V. (1964). On propagation in random media of discrete scatterers. *Proceedings of Symposia in Applied Mathematics*, XVI:84–116.

van de Hulst, H. C. (1981). *Light scattering by small particles*. Dover books on physics. Dover, New York, NY. This Dover edition, first published in 1981, is an unabridged and corrected republication of the work originally published in 1957 by John Wiley & Sons, Inc., N.Y.

Videen, G., Zubko, E., Sun, W., Shkuratov, Y., and Yuffa, A. (2015). Mixing rules and morphology dependence of the scatterer. *Journal of Quantitative Spectroscopy and Radiative Transfer*, 150:68 – 75.

Volten, H., Munoz, O., Rol, E., de Haan, J., Vassen, W., Hovenier, J., Muinonen, K., and Nousiainen, T. (2001). Scattering matrices of mineral aerosol particles at 441.6 nm and 632.8 nm. *Journal of Geophysical Research : Atmospheres*, 106(D15):17375–17401.

Waterman, P. C. (1965). Matrix formulation of electromagnetic scattering. *Proceedings of the IEEE*, 53(8):805–812.

Weidling, R., Güttler, C., and Blum, J. (2012). Free collisions in a microgravity many-particle experiment. I. Dust aggregate sticking at low velocities. *Icarus*, 218(1):688 – 700.

Williams, S. and Philipse, A. (2003). Random packings of spheres and spherocylinders simulated by mechanical contraction. *Physical review. E, Statistical, nonlinear, and soft matter physics*, 67:051301.

Yang, P., Gao, B.-C., Baum, B. A., Hu, Y. X., Wiscombe, W. J., Mishchenko, M. I., Winker, D. M., and Nasiri, S. L. (2001). Asymptotic solutions for optical properties of large particles with strong absorption. *Applied Optics*, 40(9):1532–1547.

Yang, P. and Liou, K. (2009). An "exact" geometric-optics approach for computing the optical properties of large absorbing particles. *Journal of Quantitative Spectroscopy and Radiative Transfer*, 110(13):1162 – 1177.

Yurkin, M., Maltsev, V., and Hoekstra, A. (2007). The discrete dipole approximation for simulation of light scattering by particles much larger than the wavelength. *Journal of Quantitative Spectroscopy and Radiative Transfer*, 106:546–557.

Yurkin, M. A. and Mishchenko, M. I. (2018). Volume integral equation for electromagnetic scattering: Rigorous derivation and analysis for a set of multilayered particles with piecewise-smooth boundaries in a passive host medium. *Physical Review A*, 97:043824.

Yusef-Zadeh, F., Morris, M., and White, R. L. (1984). Bipolar reflection nebulae - Monte Carlo simulations. *Astrophysical Journal*, 278:186–194.

Zurk, L. M., Tsang, L., and Winebrenner, D. P. (1996). Scattering properties of dense media from Monte Carlo simulations with application to active remote sensing of snow. *Radio Science*, 31:803–819.